

The Fredericksz transition as a bifurcation problem

G. I. Blake¹, T. Mullin¹ and S. J. Tavener²

¹*Department of Physics and Astronomy, Schuster Laboratory, Manchester University, Brunswick Street, Manchester M13 9PL, UK*

²*Department of Mathematics, Penn State University, University Park, PA 16802, USA*

(Received August 1998; final version February 1999)

Abstract. *We consider the effects of the application of electric and magnetic fields to a homogeneously aligned nematic liquid crystal which lies between parallel plates. The average alignment of the fluid molecules is known as the director and it is set parallel to the top and bottom bounding surfaces. At a critical field strength a Fredericksz transition occurs which results in a distortion of the director field. We discuss this phenomenon from the point of view of bifurcation theory and use numerical bifurcation techniques to explore it. Imperfections in the cell, either in the applied field or the director orientation at the boundaries, are also considered. Finally, we investigate the effect of finite aspect in a two-dimensional version of the problem.*

1 Introduction

The application of bifurcation theory to a variety of problems in physics and applied mathematics has led to a more complete understanding of how complicated non-linear behaviours arise in these systems (Golubitsky & Schaeffer, 1985). This approach has been successfully applied to a wide variety of problems in both fluid and solid mechanics and to chemically reacting systems. An example of this is the so-called Taylor–Couette flow of an isotropic, Newtonian fluid between concentric cylinders, for which quantitative as well as qualitative agreement between experiment, numerical computations and predictions based on bifurcation theory has been obtained, as reviewed by Mullin and Koblitz (1996). Using the governing equations for the flow of such fluids, the Navier–Stokes equations, and numerical techniques developed at AEA, Harwell, it proved possible to calculate solutions and bifurcation points which occurred as the control parameters of the problem were varied. Not only was precise quantitative agreement obtained between calculation and experiment, but also, the numerical techniques were used to uncover unstable and therefore unobservable solutions. These in turn were shown to have a direct bearing on the origins of more complicated behaviour including low-

Correspondence to T. Mullin, Department of Physics and Astronomy, Schuster Laboratory, Manchester University, Brunswick Street, Manchester M13 9PL, UK.

dimensional chaos, and the combination of theory, calculation and experiment proved to be a significant one. For many other physical situations, although the governing equations are known, they may be extremely difficult to solve in practice. Bifurcation theory may still provide insight in such cases, though it may be only qualitative and localized in nature.

In the present study we apply these powerful techniques to a nematic liquid crystal aligned uniformly between parallel plates, to which either a magnetic or electric field is applied. A nematic liquid crystal can be considered as a fluid which contains rod-like molecules which have orientational alignment without any positional order. The dielectric and magnetic properties of the material are anisotropic and we will be concerned with materials where the difference between the susceptibilities parallel and perpendicular to the molecules is positive. The average alignment of the molecules is called the director and is prescribed to be parallel to the top and bottom bounding surfaces in our work. This form of alignment is called homogeneous, whereas when the average molecular alignment is normal to the boundary, it is called homeotropic. As is well documented (see, e.g. de Gennes & Prost, 1993), at a critical value of the strength of the magnetic or electric field, a static distortion of the nematic occurs and this phenomenon is often referred to as a Freedericksz transition. It is this problem which we discuss from the perspective of bifurcation theory and demonstrate that these methods can also be applied to an anisotropic, non-Newtonian fluid.

The Freedericksz transition that occurs when a magnetic field is applied across a thin layer of a nematic confined between parallel plates has attracted considerable attention, partly due to its utility as a means of measuring elastic constants. By considering extrema of an integral expression for the free energy of the sample, both Saupe (1960) and later Dafermos (1968) determined the critical magnetic field strength above which non-trivial solutions can exist for planarly aligned nematic liquid crystals. They were also able to show that above this critical field strength the non-trivial solution in which the directors are no longer uniformly parallel to the plates is the free energy minimizer. The related problem, in which the nematic is initially aligned normal to the walls and a magnetic field is applied parallel to the walls, was shown to differ only in that the roles of the bend and splay elastic constants are reversed. Leslie (1970) confirmed these results by posing the problem in terms of the conservation of linear and angular momentum, and then applied this new approach to two different configurations. He considered the Freedericksz transition which occurs in a nematic confined in the annular gap between concentric cylinders in which the directors are initially aligned tangentially and to which a radial magnetic field is applied. He further considered the transition which occurs when a nematic is confined in a wedge with the directors initially aligned radially and to which a tangential magnetic field is applied. In each case he determined a critical field strength above which a non-trivial solution can exist and showed using the free energy of the sample, that above the critical field strength the distorted configuration is the energy minimizer. Once again, the heterogeneously aligned problem, with the magnetic field at right angles to the initial director configuration, was shown to be equivalent once the roles of splay and bend elasticity were reversed. Derfel (1988) showed that the Freedericksz transition that occurs when a magnetic field is applied normal to a nematic sample confined between parallel plates arises at a pitchfork bifurcation point. He then considered the qualitative aspects of the unfolding of this pitchfork bifurcation produced by imperfect alignment at the plates and when the magnetic field is applied at an

angle other than 90 deg to the plates. Leslie (1970) completed the trio of Freedericksz transitions between parallel plates by considering the transition which occurs when a magnetic field is applied in such a manner that its tendency to align the molecules is balanced by the elastic resistance to twist. Schiller (1989) developed a perturbation expansion for the solutions which arise beyond transition in this scenario.

The Freedericksz transition which occurs when an electric rather than a magnetic field is applied across a planarly aligned nematic sample confined in the narrow gap between two parallel plates has been examined by both Deuling (1972) and by Gruler and Meier (1972). Both studies looked for solutions which minimized a free energy and both neglected the conductivity of the sample. They not only found a critical value for the electric field above which the trivial solution loses stability to a non-uniform configuration, but successfully compared calculations of the director angle as a function of the applied field with experimental measurements of the shift in the birefringence pattern. The experimental measurements were seen to depart from the theoretical values for large voltages and for large values of the dielectric anisotropy. Gruler and Meier conjectured this departure to be the result of the non-uniform field which they could only approximate accurately for small deformations of the director field. They present plots of the non-linear electric field between the plates which are qualitatively similar to those resulting from our own finite-element computations. In common with the magnetic case, the roles of the dielectric constants parallel and perpendicular to the director and the splay and bend elastic constants are reversed when the nematic is aligned normal to the plates and the electric field is applied parallel to the plates. Deuling (1978) completed the trio of standard scenarios between parallel plates when he considered the case in which the aligning effects of an electric field are balanced by the elastic resistance to twist.

To model the behaviour of the liquid crystal we use the static continuum theory of Ericksen and Leslie (see, for example, Leslie (1992)), which we outline in the next section. In Section 3 we discuss qualitative aspects of the Freedericksz transition and in Section 4, and Appendix A, we describe the application of the finite-element method to the Freedericksz transition with an applied magnetic field. In Section 5 and Appendix B, we extend these numerical techniques to examine the analytically less tractable situation when an electric field is applied to the cell. We extend previous analyses to include the effect of mobile ions in the sample and the coupling between dielectric and conductivity anisotropies, and we investigate a fully two-dimensional version of the problem.

2 Static continuum theory for nematics

Cartesian tensor notation is used throughout, where double subscripts denote sums and commas denote differentiation with respect to the relevant spatial variables.

A vector \mathbf{n} is introduced to describe the orientation of the anisotropic axis. This vector, commonly referred to as the director, is assumed to lie parallel to the average, local orientation of the molecules and is subject to the constraint

$$n_i n_i = 1 \quad (1)$$

where \mathbf{n} is physically indistinguishable from $-\mathbf{n}$ for the non-chiral nematics considered here. Using a balance of work equation, Leslie (1992) formulates concisely the dynamic continuum theory for these materials, from which it is

relatively straightforward to deduce the static version. In this case, we simply have the equation

$$\left(\frac{\partial W}{\partial n_{ij}}\right)_{,j} - \frac{\partial W}{\partial n_i} + G_i + \gamma n_i = 0, \quad i, j = 1, 2, 3 \tag{2}$$

where W is the local stored energy function, \mathbf{G} is the external orientation body force per unit volume and γ is a Lagrange multiplier arising from the constraint (1). This equation governs the orientation of \mathbf{n} subject to elastic and external field effects.

The local stored energy function W is introduced to model elastic effects and is assumed to depend solely upon the direction \mathbf{n} and its gradients. By assuming that W depends quadratically upon the gradients of \mathbf{n} one arrives at (Frank, 1948)

$$2W = K_1(n_{ii})^2 + K_2(n_i e_{ijk} n_{kj})^2 + K_3 n_{i,p} n_p n_{i,q} n_q + (K_2 + K_4)(n_{ij} n_{ji} - (n_{ii})^2) \tag{3}$$

where the elastic coefficients, K_i , are constants at fixed temperatures and satisfy the inequalities (Ericksen, 1958)

$$K_1 > 0, \quad K_2 > 0, \quad K_3 > 0 \tag{4}$$

The constitutive equation for \mathbf{G} has different forms depending upon whether a magnetic or electric field is applied to the liquid crystal. We consider both situations and then \mathbf{G} takes the form

$$G_i = \Delta\chi H_j n_j H_i, \quad \Delta\chi = \chi_{\parallel} - \chi_{\perp} \tag{5}$$

in the case of an applied magnetic field, whilst for electric fields we have

$$G_i = \Delta\varepsilon E_j n_j E_i, \quad \Delta\varepsilon = \varepsilon_{\parallel} - \varepsilon_{\perp} \tag{6}$$

The applied magnetic and electric fields are represented through the vectors \mathbf{H} and \mathbf{E} , respectively. The constants $\Delta\chi$ and $\Delta\varepsilon$ measure the differences between the magnetic and dielectric susceptibilities parallel to the director, χ_{\parallel} and ε_{\parallel} , respectively, and perpendicular to the director, χ_{\perp} and ε_{\perp} , respectively. In general, and for all the cases considered here, $\Delta\chi$ and $\Delta\varepsilon$ are both positive.

For applied magnetic fields, equation (2) is sufficient to describe the behaviour of the nematic as the magnetic anisotropies of nematics are very small in practice, and as a result it is reasonable to assume that the effect of the material on the applied magnetic field is negligible. On the other hand, $\Delta\varepsilon$ is not generally small, so that a coupling between the liquid crystal and the applied electric field arises. Thus the liquid crystal distorts the applied electric field pattern in a way which must be calculated. Further, nematic liquid crystals possess free charges (de Gennes & Prost, 1993), so we must also take the charge density, ρ_e , of the material into consideration. We therefore need to introduce two more equations when we consider electric fields, these being Poisson's equation

$$\varepsilon_0 D_{i,i} = \rho_e \tag{7}$$

and the continuity of charge equation

$$j_{i,i} = 0 \tag{8}$$

where ε_0 is the permittivity of free space, and the electric displacement \mathbf{D} and the current density \mathbf{j} are given by

$$D_i = \varepsilon_{\perp} E_i + \Delta\varepsilon E_j n_j n_i, \quad j_i = \sigma_{\perp} E_i + \Delta\sigma E_j n_j n_i, \quad \Delta\sigma = \sigma_{\parallel} - \sigma_{\perp} \tag{9}$$

where σ_{\parallel} and σ_{\perp} are the conductivities of the material parallel and perpendicular to the director, respectively (see Kaiser & Pesch, 1993). The electric field is of course subject to the constraint

$$e_{ijk}E_{k,j} = 0 \tag{10}$$

where the third-order tensor \mathbf{e} is the alternator.

Our approach extends that of previous studies (for a review see Dunmur & Toriyama, 1998) which do not allow for the presence of mobile ions in the sample and assume instead that $D_{i,ji} = 0$. This simplification allows the free-energy minimization problem to be reduced to a suitably scaled version of the problem when a magnetic field is applied (see, e.g. de Gennes & Prost, 1993, p. 135). Our numerical techniques permit the exploration of the coupling between the director, the local charge density and the electrical field.

3 The Freedericksz transition

We consider a nematic liquid crystal confined between parallel plates and uniformly aligned so that the director is everywhere perfectly parallel to the surfaces, as shown schematically in Fig. 1.

It is well known that if a magnetic field is applied perpendicular to the plates, or a potential difference is applied across them, a distortion of the nematic alignment occurs above a critical magnetic or electric field strength provided the magnetic or dielectric anisotropies are positive. In other words, below the critical field strength the director profile is unperturbed and remains uniform, but above this value a distortion occurs. This effect is due to a competition between restoring elastic forces induced by the alignment at the boundaries and destabilizing torques produced by the external field. The external field produces destabilizing torques since the nematic materials we consider have positive magnetic or dielectric anisotropies, promoting the director to lie parallel to the direction of the applied field. Below the critical field strength the destabilizing torques are insufficient to overcome the elastic forces and the director profile remains uniform. However, above this critical field strength, the torques arising due to magnetic or electric anisotropies overcome the elastic forces and the director profile becomes distorted. This phenomenon is commonly known as a Freedericksz transition.

The Freedericksz transition can be considered as an example of a symmetry breaking (pitchfork) bifurcation. The symmetry being broken is a reflectional (anti)symmetry about the mid-plane. Other examples of such bifurcations are discussed in Mullin (1995). In our problem, let the angle which the director in the

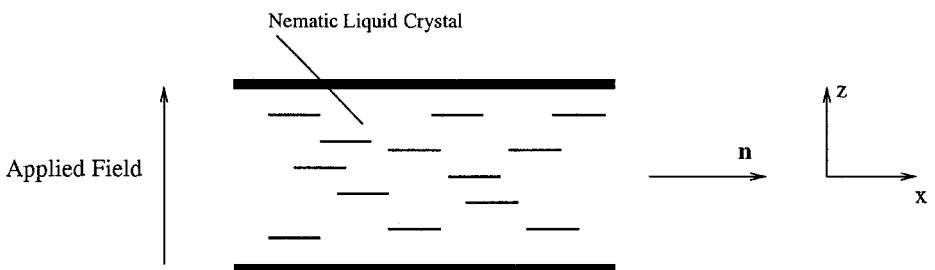


Fig. 1. Schematic for the Freedericksz transition.

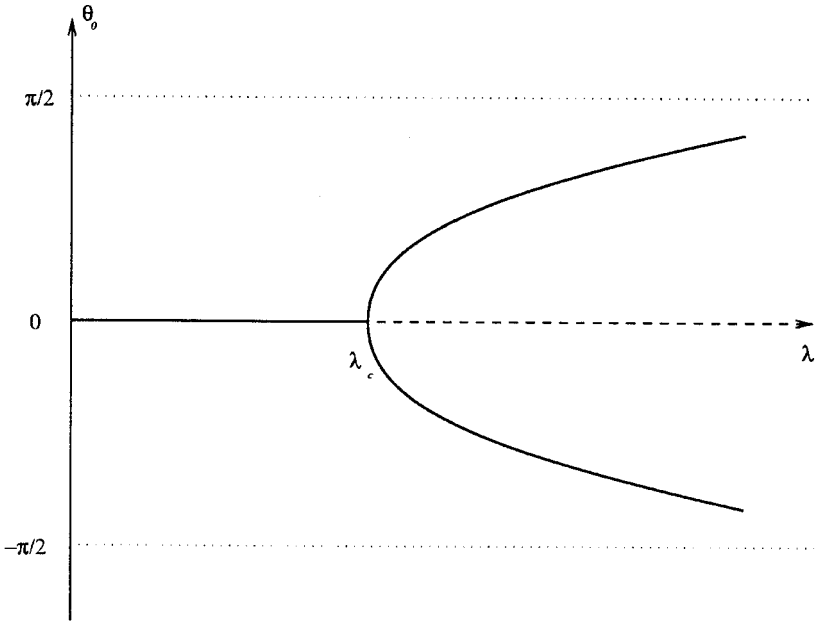


Fig. 2. A pitchfork bifurcation diagram.

centre of the cell makes with the plates be denoted by θ_0 and the field strength by λ . Then $\theta_0 = 0$ for $\lambda < \lambda_c$, say, as shown schematically in Fig. 2. At $\lambda = \lambda_c$ two non-trivial solutions appear corresponding to clockwise and anticlockwise rotations of the director, both of which are stable. The trivial solution becomes an unstable solution of the equilibrium equations at this point and a distortion in the director field occurs. In other words, as we increase the parameter λ steadily from zero, the trivial solution exchanges stability with one or two possible non-trivial solutions at $\lambda = \lambda_c$. Note that due to the symmetry of this idealized, perfect cell about the central plane parallel to the bounding surfaces, either of the clockwise or anticlockwise distortions are equally likely to occur, and the bifurcation is a pitchfork. Figure 2 illustrates the exchange of stability between the undistorted and distorted states, the dashed line representing the fact that the situation $\theta_0 = 0$ is still a possible configuration for $\lambda > \lambda_c$, but an unstable one. The distorted solution branches approach either $\pi/2$ or $-\pi/2$ in the limit as $\lambda \rightarrow \infty$.

In the following sections we show numerically that the qualitative description of the Freedericksz transition applies equally to the magnetic and electric field cases. We also discuss the more physically relevant case where the symmetry about the central plane of the cell is broken. As is well known from singularity theory, imperfections which arise naturally in physical systems can be modelled mathematically independently of the precise nature of the imperfection. In our computations we consider the effects of a non-perpendicular field in the magnetic case and imperfect anchoring in the electrical one.

4 Application of a magnetic field

In this section we consider the liquid crystal cell just described, to which a magnetic field is applied at a fixed angle, ψ , to the normal of the plates. The direction of the

field is assumed to lie in the plane perpendicular to the plates which contains the undistorted director profile. That is

$$\mathbf{H} = H(\sin \psi, 0, \cos \psi), \quad -\frac{\pi}{2} < \psi < \frac{\pi}{2} \tag{11}$$

where the x -axis is defined to be parallel to the plates and the undistorted director configuration and the z -axis is perpendicular to the plates. Two cases will be discussed: $\psi = 0$ and $\psi \neq 0$. In the first case the problem has a reflectional symmetry about the mid-plane of the cell, but for finite values of ψ this symmetry is broken. This latter instance is of more practical significance, as in any experiment of this type the magnetic field will always be at some non-zero angle to the normal of the plates.

We assume that distortions in the director profile caused by the application of such a magnetic field are entirely uniform in planes parallel to the plates and therefore seek solutions of the form

$$\mathbf{n} = (\cos \theta, 0, \sin \theta), \quad \theta = \theta(z) \tag{12}$$

The constraint (1) is satisfied automatically. From (2), (3), (5) and (11) we then have

$$-K_3 \left(\frac{d^2 \theta}{dz^2} \sin \theta + 3 \left(\frac{d\theta}{dz} \right)^2 \cos \theta \right) \sin^2 \theta + \Delta \chi H^2 \sin(\theta + \psi) \sin \psi + \gamma \cos \theta = 0 \tag{13}$$

$$\begin{aligned} & K_1 \left(\frac{d^2 \theta}{dz^2} \cos \theta - \left(\frac{d\theta}{dz} \right)^2 \sin \theta \right) \\ & + K_3 \left(\frac{d^2 \theta}{dz^2} \sin \theta \cos \theta + \left(\frac{d\theta}{dz} \right)^2 \cos 2\theta - \left(\frac{d\theta}{dz} \right)^2 \sin^2 \theta \right) \sin \theta \\ & + \Delta \chi H^2 \sin(\theta + \psi) \cos \psi + \gamma \sin \theta = 0 \end{aligned} \tag{14}$$

and upon elimination of γ

$$\begin{aligned} & K_1 \left(\frac{d^2 \theta}{dz^2} \cos \theta - \left(\frac{d\theta}{dz} \right)^2 \sin \theta \right) \cos \theta + K_3 \left(\frac{d^2 \theta}{dz^2} \sin \theta + \left(\frac{d\theta}{dz} \right)^2 \cos \theta \right) \sin \theta \\ & + \Delta \chi H^2 \sin(\theta + \psi) \cos(\theta + \psi) = 0 \end{aligned} \tag{15}$$

We specify that strong anchoring conditions hold at the boundaries, that is the director is not free to move at the plates. Taking the x -axis to be equidistant and parallel to the bounding surfaces and the gap between the plates as d , the boundary conditions read

$$\theta(-d/2) = \theta(d/2) = 0 \tag{16}$$

We note for future reference that when $\psi = 0$ the trivial solution

$$\theta(z) = 0 \tag{17}$$

is a solution of (15) subject to (16) for all field strengths H . However, there is no such trivial solution for non-zero ψ .

4.1 Numerical method

The results we present in the following sections have all been obtained using the numerical package ENTWIFE (Cliffe, 1996), which has been developed at AEA, Harwell. The package utilizes the finite-element method to solve systems of non-linear partial and ordinary differential equations and implements modern numerical continuation and bifurcation algorithms.

We first recast (15) in weak form. Multiplying (15) by a test function $\Theta(z)$ which vanishes at $z = \pm d/2$, then integrating by parts over the interval $[-d/2, d/2]$ we arrive at

$$\int_{-d/2}^{d/2} \left\{ \left[(K_3 - K_1) \left(\frac{d\theta}{dz} \right)^2 \sin \theta \cos \theta + \Delta\chi H^2 \sin(\theta + \psi) \cos(\theta + \psi) \right] \Theta - (K_1 \cos^2 \theta + K_3 \sin^2 \theta) \frac{d\theta}{dz} \frac{d\Theta}{dz} \right\} dz = 0 \tag{18}$$

We non-dimensionalize this equation by introducing the new variable

$$\tilde{z} = \frac{z}{d} \tag{19}$$

and multiplying through by d^2/K_1 , to obtain

$$\int_{-1/2}^{1/2} \left\{ \left[(\mu - 1) \left(\frac{d\theta}{d\tilde{z}} \right)^2 \sin \theta \cos \theta + \lambda \sin(\theta + \psi) \cos(\theta + \psi) \right] \Theta - (\cos^2 \theta + \mu \sin^2 \theta) \frac{d\theta}{d\tilde{z}} \frac{d\Theta}{d\tilde{z}} \right\} d\tilde{z} = 0 \tag{20}$$

where

$$\mu = \frac{K_3}{K_1} \text{ and } \lambda = \frac{\Delta\chi H^2 d^2}{K_1} \tag{21}$$

From (4), μ is positive. We find that this parameter does not have any marked effect on what follows, changing the quantitative but not the qualitative nature of the solutions. As a result we assume that μ is unity, i.e. $K_1 = K_3$, throughout.

There are now two main parameters in our problem which we are free to vary. These are λ and ψ . We vary λ and associate an increase or decrease of λ with a corresponding increase or decrease of H^2 . We thus assume that $\Delta\chi$, d and K_1 are fixed. We also regard ψ as being free to vary, but usually consider a specific value of this parameter. In the nomenclature of bifurcation theory, λ and ψ are the distinguished and secondary parameters, respectively.

A finite-element discretization of (18) as described briefly in Appendix A, results in a finite-dimensional algebraic system of equations

$$\mathbf{f}(\mathbf{u}, \lambda) = \mathbf{0}, \quad \mathbf{f} : \mathbb{R}^N \times \mathbb{R} \mapsto \mathbb{R}^N$$

where \mathbf{u} is the vector containing the coefficients of the N basis functions $\psi_i(\tilde{z})$ and defines the finite-element approximation $\theta_h(\tilde{z})$ of $\theta(\tilde{z})$ via equation (A16). If (and

only if), $\psi = 0$ and the finite-element grid is symmetric about $z = 0$, this non-linear system of equations is equivariant with respect to an orthogonal matrix \hat{S} , i.e.

$$\mathbf{f}(\hat{S}\mathbf{u}, \lambda) = \hat{S}\mathbf{f}(\mathbf{u}, \lambda)$$

where $\hat{S} \neq I$ and $\hat{S}^2 = I$. Details appear in Appendix A. The orthogonal matrix \hat{S} induces a unique decomposition of \mathbb{R}^N into symmetric and antisymmetric subspaces

$$\mathbb{R}^N = \mathbb{R}_s^N \oplus \mathbb{R}_a^N$$

where

$$\mathbb{R}_s^N = \{\mathbf{u} \in \mathbb{R}^N : \hat{S}\mathbf{u} = \mathbf{u}\}$$

and

$$\mathbb{R}_a^N = \{\mathbf{u} \in \mathbb{R}^N : \hat{S}\mathbf{u} = -\mathbf{u}\}$$

At a simple symmetry-breaking bifurcation point $(\mathbf{u}_c, \lambda_c)$

$$\mathbf{u}_c \in \mathbb{R}_s^N$$

$$\text{Null}(\mathbf{f}_\mathbf{u}^c) = \text{span}\{\mathbf{a}\}, \quad \mathbf{a} \in \mathbb{R}_a^N, \mathbf{a} \neq \mathbf{0}$$

$$\text{Range}(\mathbf{f}_\mathbf{u}^c) = \{\mathbf{y} \in \mathbb{R}^N : \psi^T \mathbf{y} = 0\}, \quad \psi \in \mathbb{R}^N, \psi \neq \mathbf{0}$$

where

$$\mathbf{f}_\mathbf{u}^c = \frac{\partial \mathbf{f}}{\partial \mathbf{u}}(\mathbf{u}_c, \lambda_c)$$

The Freedericksz transition occurs at such a symmetry-breaking bifurcation point and was computed as a regular solution of the extended system described by Werner and Spence (1984), namely

$$\mathbf{F}(\mathbf{v}) = \begin{pmatrix} \mathbf{f} \\ \mathbf{f}_\mathbf{u} \mathbf{a} \\ \mathbf{1}^T \mathbf{a} - 1 \end{pmatrix} = \mathbf{0} \tag{22}$$

where

$$\mathbf{v}^T = (\mathbf{u}^T, \mathbf{a}^T, \lambda), \quad \mathbf{v} \in (\mathbb{R}_s^N \times \mathbb{R}_a^N \times \mathbb{R}^1)$$

$$\mathbf{F} : \mathbb{R}_s^N \times \mathbb{R}_a^N \times \mathbb{R}^1 \rightarrow \mathbb{R}_s^N \times \mathbb{R}_a^N \times \mathbb{R}^1$$

and $\mathbf{1} \in \mathbb{R}^N$ with $\mathbf{1} \neq \mathbf{0}$.

4.2 A perfect pitchfork bifurcation

When $\psi = 0$ the magnetic field is perpendicular to the plates and the governing equations are equivariant with respect to a reflection about $z = 0$. In this case a Freedericksz transition occurs at a critical strength of the magnetic field at a symmetry breaking bifurcation point. Equation (22) was solved using a finite-element mesh on the interval $z \in [-1/2, 0]$ comprised of one-dimensional elements with quadratic interpolation within each element. A convergence study is shown in

Table 1. The location of the numerically determined bifurcation point $\bar{\lambda}_c$, and the relative error E , using N elements with quadratic interpolation within each element

No. of elements, N	Bifurcation point, $\bar{\lambda}_c$	Relative error, E	Ratio, $E(N)/E(N/2)$
2	9.874659026	5.1214×10^{-4}	—
4	9.869927789	3.2766×10^{-5}	6.3979×10^{-2}
8	9.869624735	2.0603×10^{-6}	6.2879×10^{-2}
16	9.869605674	1.2897×10^{-7}	6.2598×10^{-2}
32	9.869604481	8.0956×10^{-9}	6.2771×10^{-2}
64	9.869604406	4.9647×10^{-10}	6.1326×10^{-2}
128	9.869604401	1.0132×10^{-11}	2.0408×10^{-2}
256	9.869604401	1.0132×10^{-11}	1.0

Table 1. The theoretical value is $\lambda_c = \pi^2$ (see de Gennes & Prost, 1993, p. 128) and the relative error is defined as $|\bar{\lambda}_c - \lambda_c|/\lambda_c$. It can be seen that the relative error converges to zero with rate $O(h^4)$ where h is the mesh spacing. A convergence criterion of 10^{-12} was used.

The computed bifurcation diagram for the Freedericksz transition is shown in Fig. 3, which is a plot of the angle of deflection of the director with respect to the plates in the centre of the cell against the parameter λ . The upper branch corresponds to an anticlockwise rotation of the director towards the applied field while the lower branch corresponds to a clockwise rotation. Note that as λ increases, the branches tend towards $\pm\pi/2$ as expected.

The calculated director profiles $\theta(z)$ corresponding to the upper branch of the

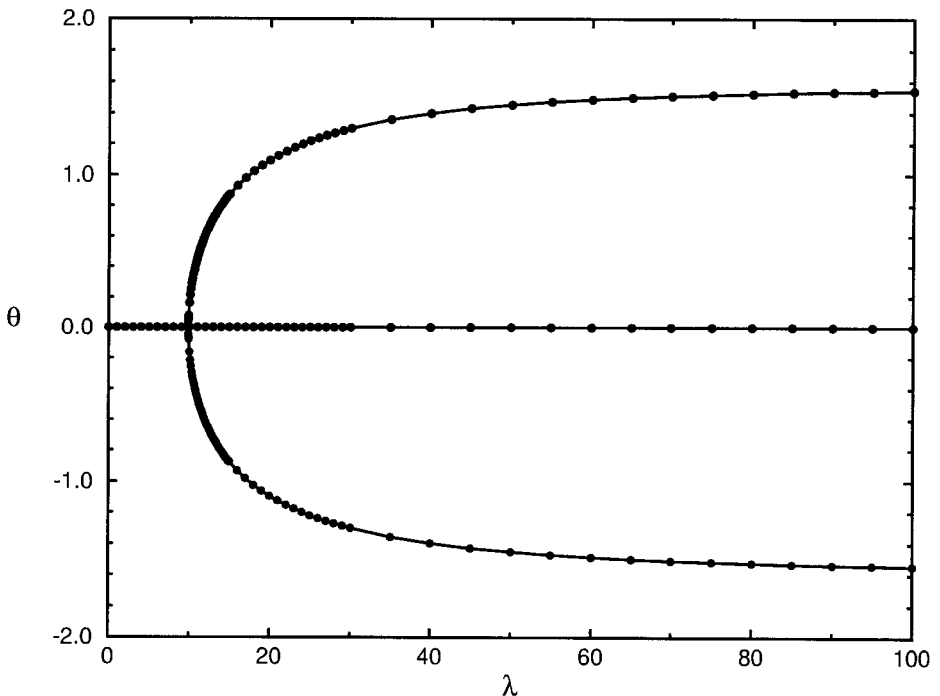


Fig. 3. Computed bifurcation diagram for an applied magnetic field with $\psi = 0$.

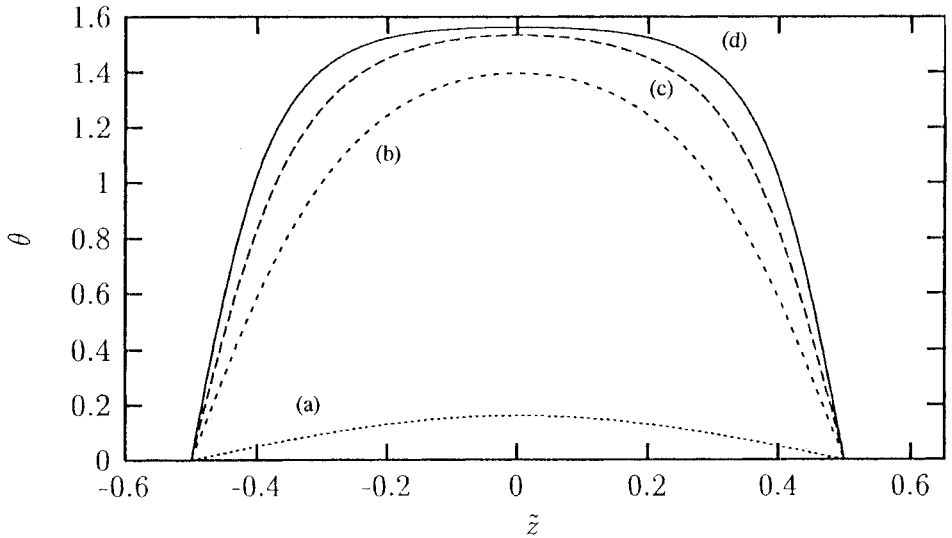


Fig. 4. Director profiles $\theta(z)$ on the upper branch: (a) $\lambda = 10$; (b) $\lambda = 40$; (c) $\lambda = 90$; (d) $\lambda = 160$.

bifurcation diagram are shown in Fig. 4 for $\lambda = 10, 40, 90$ and 160 . These solutions were calculated using a grid of 160 elements on the interval $z \in [-1/2, 1/2]$. The parameter value $\lambda = 10$ is just past the bifurcation point and the associated solution is a slight perturbation of the trivial solution and is essentially sinusoidal in shape. The other parameter values correspond to approximately two, three and four times the critical field strength at which the Freedericksz transition occurs. It can be seen that a greater proportion of the nematic is aligned in the direction of the field as λ increases and the shape is far from sinusoidal.

4.3 A disconnected pitchfork bifurcation

The perfect pitchfork bifurcation described in the last section is of course a mathematical abstraction which can never be realized in any practical situation, as any experiment contains imperfections. These imperfections come from many sources, for example, non-perfect alignment of the liquid crystal, non-parallel plates and imperfections in the material. We have introduced the angle ψ , the amount by which the direction of the applied magnetic field deviates from the normal to the plates, to model the effect of imperfections on the behaviour of the Freedericksz cell. The theory of imperfect bifurcations (Golubitsky & Schaeffer, 1985) tells us that it is reasonable to model possibly multiple and complicated imperfections in this manner.

The trivial solution $\theta(z) = 0$ is now no longer a solution for $\lambda \geq 0$ and a distortion occurs for any value of λ . The computed bifurcation diagram with $\psi = 0.02$ rad, approximately 1 deg, is shown in Fig. 5. The axes are the same as in the previous bifurcation diagram. It is immediately obvious that the perfect pitchfork of the previous section has become disconnected. The upper branch is known as the primary solution branch (Benjamin, 1978) and indicates that there is a distortion of the director profile even in the absence of an applied field. For λ increasing steadily from zero, the primary solution, corresponding to anticlockwise rotation

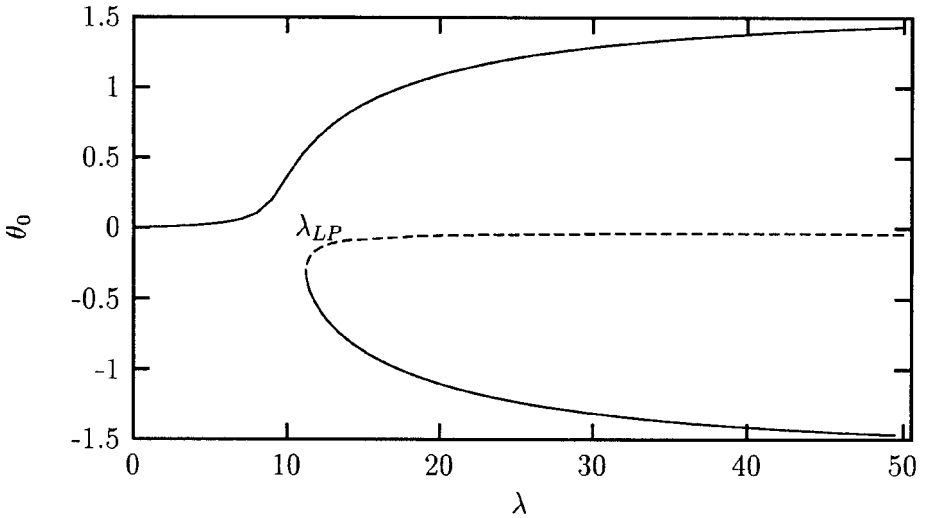


Fig. 5. Bifurcation diagram for an imperfect Freedericksz experiment with $\psi = 0.02$.

of the director, is the only one available to the cell. This branch is straightforward to calculate and is achieved by gradually increasing the value of the distinguished parameter λ . Two other solutions exist for λ sufficiently large and cannot be reached by a smooth increase in field strength. The solution associated with the top part of the lower, disconnected branch is unstable and therefore unobservable. The bottom part of the lower, disconnected branch is a stable solution but one which can only be reached by suddenly switching on the magnetic field.

The disconnected branch can be computed by setting ψ to zero and increasing the distinguished parameter to some value greater than λ_c , meanwhile ensuring that the solution remains on the trivial branch. Upon increasing ψ from zero we remain on the unstable part of the now disconnected bifurcation diagram. Keller arclength continuation (Keller, 1977) can then be used to find the other points on the disconnected branch.

For negative values of ψ the situation is reversed and the primary solution branch corresponds to clockwise rotations of the director and the disconnected branch to anticlockwise rotations. The bifurcation diagram for $\psi = -0.02$ is simply a reflection of Fig. 5 about the λ -axis.

The calculated stable director profiles $\theta(\tilde{z})$ are shown in Fig. 6 for the connected and disconnected branches when $\lambda = 50$ and $\psi = 0.02$ rad. The disconnected branch at this value of ψ only exists for $\lambda > \lambda_{LP} = 11.21$. Once the cell is in a state corresponding to the stable part of the disconnected branch and the field strength is reduced continuously, the magnitude of the clockwise rotation decreases continuously until at the limit point where $\lambda = \lambda_{LP}$ the cell returns catastrophically to the anticlockwise solution branch. As ψ is increased or decreased the disconnection between the two solution branches increases or decreases, respectively, and the position of the limit point also varies as a consequence. The computed locus of limit points is shown as a function of the secondary parameter ψ in Fig. 7. The location of the limit point can be computed as ψ is varied using the extended system described by Moore and Spence (1980). The curve is a cusp which is aligned with the λ -axis with vertical asymptotes at $\psi = \pm \pi/2$, and results from an

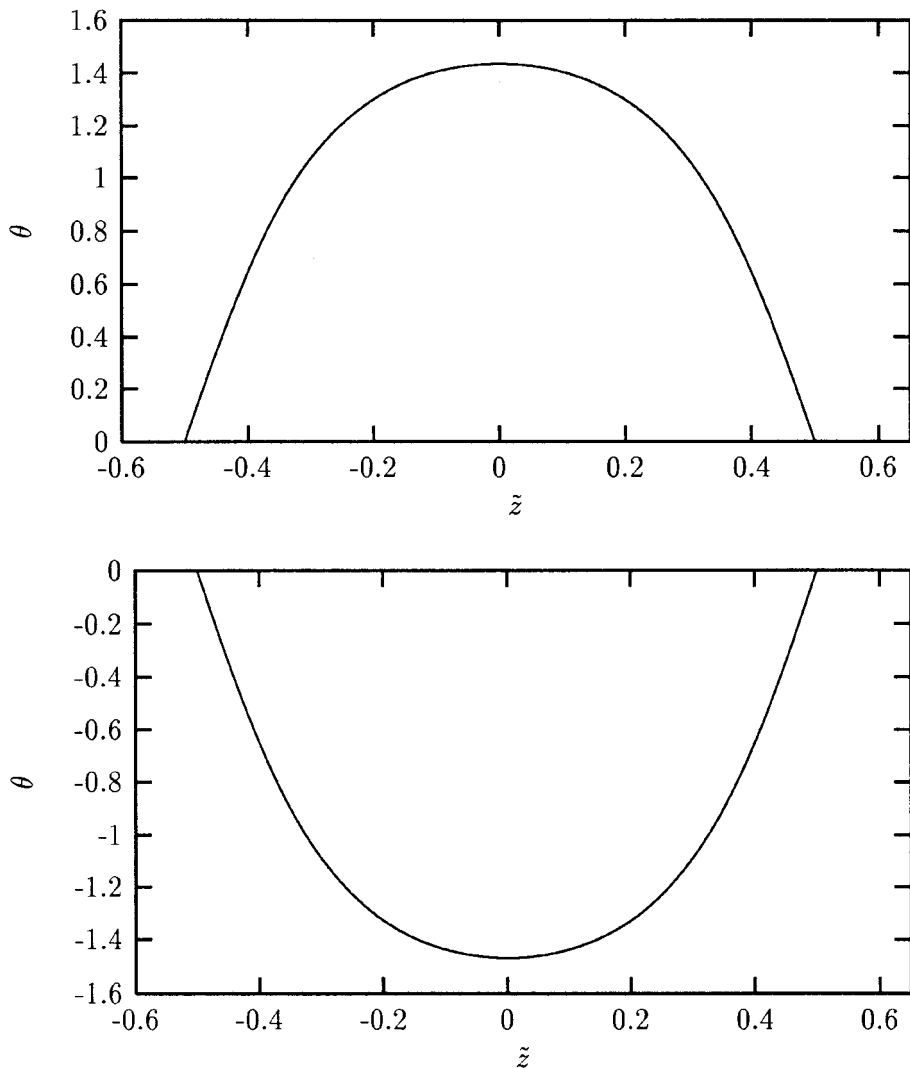


Fig. 6. Director profiles $\theta(\tilde{z})$ for $\lambda = 50$ and $\psi = 0.02$: (a) primary branch; (b) disconnected branch.

unfolding of the pitchfork. The qualitative nature of the unfolding of the pitchfork bifurcation for small imperfections has been described previously by Derfel (1988) who performed a normal form analysis. A similar result to this has previously been obtained in Rayleigh–Bénard convection (Cliffe & Winters, 1984) in Newtonian fluids which conform to the Boussinesq approximation, where a tilt of the convection cell provided the unfolding parameter.

5 Application of an electric field

Now that we have illustrated how ideas from bifurcation theory can be applied to the simple Freedericksz transition with respect to a magnetic field, we move on to discuss the more complicated situation where an electric field is applied. In this case, instead of a single variable, namely the angle the director makes with the

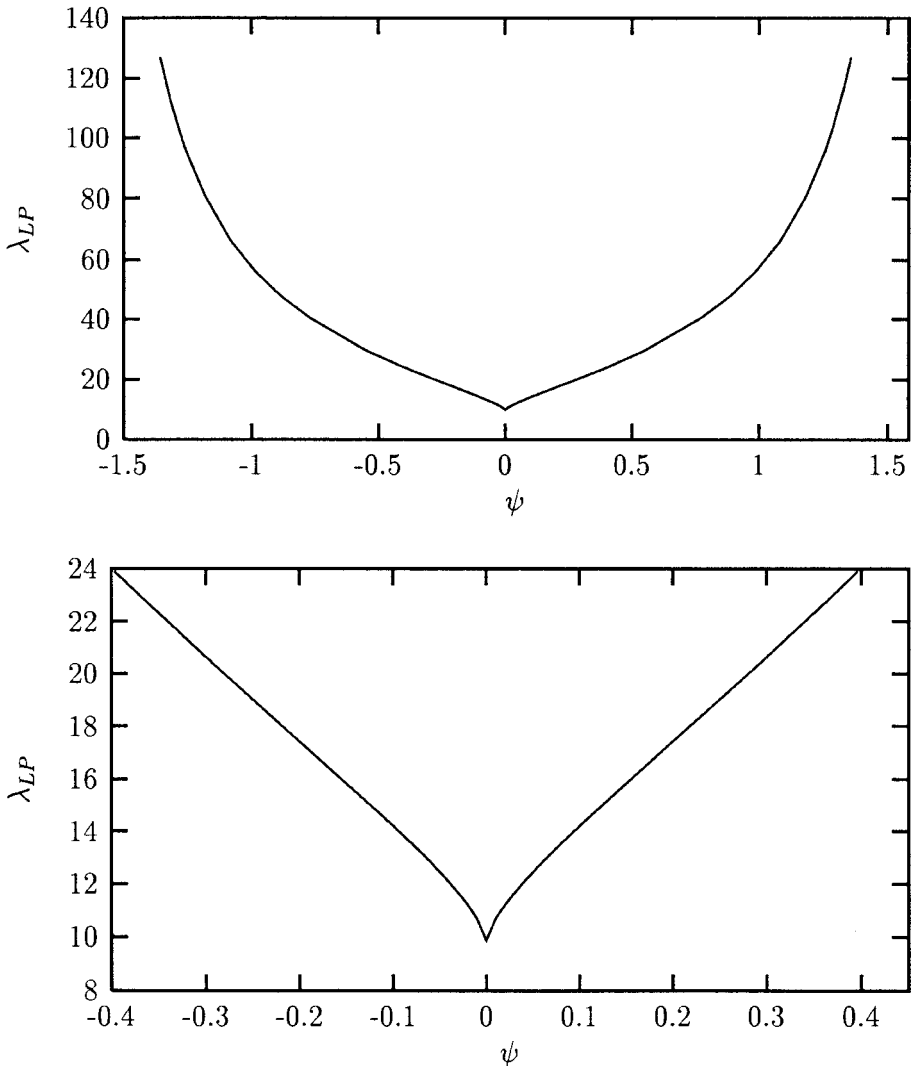


Fig. 7. (a) Locus of limit points λ_{LP} on the disconnected branch. (b) Tip of the cusp.

plates, the variation of the electric field and the charge density in the sample must also be taken into consideration. We also introduce a second spatial dimension into the problem and demonstrate that the ideas we presented in the previous section for an ODE apply equally well for a system of partial differential equations. To this end we allow the variables to depend upon x as well as z , the x -axis being associated with the direction the director is pointing in before the electric field is applied (see Fig. 1). It is assumed that in the experiment, the nematic is a perfect insulator containing mobile charges and that the sample is separated from the electrodes by, for example, suitable insulating layers to eliminate charge injection.

To satisfy the constraint (10) we assume that \mathbf{E} can be expressed as

$$\mathbf{E} = \left(-\frac{\partial\phi}{\partial x}, 0, -\frac{\partial\phi}{\partial z} \right), \quad \phi = \phi(x, z) \quad (23)$$

and then the three variables in our problem are the electric potential, ϕ , the charge density, ρ_e , and θ , the angle the director makes with the plates. All these variables are assumed to be functions of x and z . Again, elastic effects contribute towards the quantitative rather than the qualitative behaviour of the system and so we set $K_1 = K_3 = K$.

With (12) (where now $\theta = \theta(x, z)$) and (23) as our ansatz for \mathbf{n} and \mathbf{E} , we obtain the governing equations

$$-K \left(\frac{\partial^2 \theta}{\partial x^2} + \frac{\partial^2 \theta}{\partial z^2} \right) + \Delta \varepsilon \left(\frac{\partial \phi}{\partial x} \cos \theta + \frac{\partial \phi}{\partial z} \sin \theta \right) \left(\frac{\partial \phi}{\partial x} \sin \theta - \frac{\partial \phi}{\partial z} \cos \theta \right) = 0 \quad (24)$$

$$- \varepsilon_{\perp} \left(\frac{\partial^2 \phi}{\partial x^2} + \frac{\partial^2 \phi}{\partial z^2} \right) - \Delta \varepsilon \frac{\partial}{\partial x} \left(\left(\frac{\partial \phi}{\partial x} \cos \theta + \frac{\partial \phi}{\partial z} \sin \theta \right) \cos \theta \right) \quad (25)$$

$$- \Delta \varepsilon \frac{\partial}{\partial z} \left(\left(\frac{\partial \phi}{\partial x} \cos \theta + \frac{\partial \phi}{\partial z} \sin \theta \right) \sin \theta \right) = \frac{\rho_e}{\varepsilon_0}$$

$$- \sigma_{\perp} \left(\frac{\partial^2 \phi}{\partial x^2} + \frac{\partial^2 \phi}{\partial z^2} \right) - \Delta \sigma \frac{\partial}{\partial x} \left(\left(\frac{\partial \phi}{\partial x} \cos \theta + \frac{\partial \phi}{\partial z} \sin \theta \right) \cos \theta \right) \quad (26)$$

$$- \Delta \sigma \frac{\partial}{\partial z} \left(\left(\frac{\partial \phi}{\partial x} \cos \theta + \frac{\partial \phi}{\partial z} \sin \theta \right) \sin \theta \right) = 0$$

from (2), (3), (6), (7) and (8).

We assume the plates to have length l in the x -direction and that a constant potential difference is applied at the plates which are perfect conductors, and hence

$$\phi(x, -d/2) = -\phi_0/2, \quad \phi(x, d/2) = \phi_0/2, \quad \rho_e(x, -d/2) = \rho_e(x, d/2) = 0, \quad -l/2 \leq x \leq l/2 \quad (27)$$

where $\phi_0 > 0$ is the voltage. (The motivation for this particular choice of boundary conditions for ϕ will become apparent in Section 5.1 where we show that this choice supports a ‘trivial’ solution for which the electric potential $\phi(x, z)$ is an odd function of z , and the trivial solution is therefore symmetric with respect to the Z_2 -reflection symmetry defined in equation (B3)).

Initially we assume that the director is strongly anchored at the boundaries so that it is parallel to the plates. That is

$$\theta(x, -d/2) = \theta(x, d/2) = 0, \quad -l/2 \leq x \leq l/2 \quad (28)$$

First we impose stress-free boundary conditions of the form

$$\begin{aligned} \frac{\partial \theta}{\partial x}(-l/2, z) &= \frac{\partial \rho_e}{\partial x}(-l/2, z) = \frac{\partial \phi}{\partial x}(-l/2, z) \\ &= \frac{\partial \theta}{\partial x}(l/2, z) = \frac{\partial \rho_e}{\partial x}(l/2, z) = \frac{\partial \phi}{\partial x}(l/2, z) = 0 \end{aligned} \quad (29)$$

for $-d/2 < z < d/2$.

This boundary value problem is again recast in weak form by first multiplying

each of (24), (25) and (26) by test functions $\Theta(x, z)$, $\Psi(x, z)$ and $\Phi(x, z)$ which satisfy

$$\Theta(x, -d/2) = \Theta(x, d/2) = \Psi(x, -d/2) = \Psi(x, d/2) = \Phi(x, -d/2) = \Phi(x, d/2) = 0 \quad (30)$$

for $-l/2 \leq x \leq l/2$, and integrating over the $(x, z) \in [-l/2, l/2] \times [-d/2, d/2]$. Introducing the non-dimensional variables

$$\bar{x} = \frac{x}{l}, \quad \bar{z} = \frac{z}{d}, \quad \bar{\phi} = \frac{\phi}{\phi_0}, \quad \bar{\rho}_e = \frac{d^2}{\varepsilon_0 \varepsilon_{\perp} \phi_0} \rho_e \quad (31)$$

and the parameters

$$\lambda = \frac{\varepsilon_{\perp} \phi_0^2}{K}, \quad \varepsilon = \frac{\varepsilon_{\parallel}}{\varepsilon_{\perp}} - 1, \quad \sigma = \frac{\sigma_{\parallel}}{\sigma_{\perp}} - 1, \quad \Gamma = \frac{d}{l} \quad (32)$$

and integrating by parts as appropriate, we find the weak forms of (24), (25) and (26) to be

$$\int_{-1/2}^{1/2} \int_{-1/2}^{1/2} \left[\left(\Gamma^2 \frac{\partial \theta}{\partial \bar{x}} \frac{\partial \Theta}{\partial \bar{x}} + \frac{\partial \theta}{\partial \bar{z}} \frac{\partial \Theta}{\partial \bar{z}} \right) + \varepsilon \lambda \left(\Gamma^2 \frac{\partial \phi}{\partial \bar{x}} \cos \theta + \frac{\partial \phi}{\partial \bar{z}} \sin \theta \right) \left(\Gamma^2 \frac{\partial \phi}{\partial \bar{x}} \sin \theta - \frac{\partial \phi}{\partial \bar{z}} \cos \theta \right) \Theta \right] d\bar{x} d\bar{z} = 0 \quad (33)$$

$$\int_{-1/2}^{1/2} \int_{-1/2}^{1/2} \left[\bar{\rho}_e \Psi - \left(\Gamma^2 \frac{\partial \phi}{\partial \bar{x}} \frac{\partial \Psi}{\partial \bar{x}} + \frac{\partial \phi}{\partial \bar{z}} \frac{\partial \Psi}{\partial \bar{z}} \right) - \varepsilon \left(\Gamma^2 \frac{\partial \phi}{\partial \bar{x}} \cos \theta + \Gamma \frac{\partial \phi}{\partial \bar{z}} \sin \theta \right) \cos \theta \frac{\partial \Psi}{\partial \bar{x}} - \varepsilon \left(\Gamma \frac{\partial \phi}{\partial \bar{x}} \cos \theta + \frac{\partial \phi}{\partial \bar{z}} \sin \theta \right) \sin \theta \frac{\partial \Psi}{\partial \bar{z}} \right] d\bar{x} d\bar{z} = 0 \quad (34)$$

$$\int_{-1/2}^{1/2} \int_{-1/2}^{1/2} \left[\Gamma^2 \frac{\partial \phi}{\partial \bar{x}} \frac{\partial \Phi}{\partial \bar{x}} + \frac{\partial \phi}{\partial \bar{z}} \frac{\partial \Phi}{\partial \bar{z}} \right] + \sigma \left(\Gamma^2 \frac{\partial \phi}{\partial \bar{x}} \cos \theta + \Gamma \frac{\partial \phi}{\partial \bar{z}} \sin \theta \right) \cos \theta \frac{\partial \Phi}{\partial \bar{x}} + \sigma \left(\Gamma \frac{\partial \phi}{\partial \bar{x}} \cos \theta + \frac{\partial \phi}{\partial \bar{z}} \sin \theta \right) \sin \theta \frac{\partial \Phi}{\partial \bar{z}} \right] d\bar{x} d\bar{z} = 0 \quad (35)$$

The boundary conditions (27), (28) and (29) become

$$\bar{\phi}(\bar{x}, -1/2) = -1/2, \quad \bar{\phi}(\bar{x}, 1/2) = 1/2, \quad \bar{\rho}_e(\bar{x}, -1/2) = \bar{\rho}_e(\bar{x}, 1/2) = 0 \quad (36)$$

$$\theta(\bar{x}, -1/2) = \theta(\bar{x}, 1/2) = 0 \quad (37)$$

$$\begin{aligned} \frac{\partial \theta}{\partial \bar{x}}(-1/2, \bar{z}) &= \frac{\partial \bar{\rho}_e}{\partial \bar{x}}(-1/2, \bar{z}) = \frac{\partial \bar{\phi}}{\partial \bar{x}}(-1/2, \bar{z}) = \frac{\partial \theta}{\partial \bar{x}}(1/2, \bar{z}) \\ &= \frac{\partial \bar{\rho}_e}{\partial \bar{x}}(1/2, \bar{z}) = \frac{\partial \bar{\phi}}{\partial \bar{x}}(1/2, \bar{z}) = 0 \end{aligned} \quad (38)$$

where $-1/2 \leq \tilde{x} \leq 1/2$ and $-1/2 < \tilde{z} < 1/2$. The ‘natural’ boundary conditions (38) arise from the integration by parts used in deriving (33), (34) and (35).

This boundary value problem was solved using the finite-element method on a grid comprising quadrilateral elements with biquadratic interpolation of all the variables within each element. We regard λ as the distinguished parameter and ε as the secondary parameter. Symmetry considerations are presented in Appendix B.

5.1 Pitchfork bifurcation

The set of boundary conditions (27), (28) and (29) allows a trivial solution

$$\theta(x, z) = 0, \quad \vec{\phi}(x, z) = z, \quad \tilde{\rho}_e(x, z) = 0, \quad -1/2 \leq x \leq 1/2, \quad -d/2 \leq z \leq d/2 \quad (39)$$

for (24), (25) and (26) for all values of λ . This solution has reflectional (anti)symmetry about the line $z = 0$ and we found the behaviour of the system to be similar to that of the corresponding magnetic field problem of Section 4.1. That is, by setting ε , σ and Γ to some fixed, physically meaningful values, we found that for λ less than λ_c the trivial solution given by (39) is stable, but at λ_c a pitchfork bifurcation occurs and this solution exchanges stability with two non-trivial solutions. Again these non-trivial solutions correspond to clockwise and anticlockwise rotations of the director towards the direction of the applied field. A bifurcation diagram was plotted and found to be qualitatively similar to Fig. 3. Our non-dimensionalization introduces a known relationship (see de Gennes & Prost, 1993, p. 135) between the value of λ_c and ε , that is

$$\lambda_c = \frac{\pi^2}{\varepsilon} \quad (40)$$

The inclusion of sample conductivity and the presence of free ions does not affect the critical field strength for the Freedericksz transition due to a decoupling which occurs when linearizing about the trivial solution. In Fig. 8 the computed values of λ_c at discrete values of ε are shown as solid circles and the theoretical value is given as the solid curve. The close correspondence between the numerical and analytical results provides confidence in our computational procedures.

The calculations of the symmetry breaking bifurcation point were performed on the grid $(\tilde{x}, \tilde{z}) \in [-1/2, 1/2] \times [-1/2, 0]$. Solutions along the stable branches for $\lambda > \lambda_c$ were calculated $(\tilde{x}, \tilde{z}) \in [-1/2, 1/2] \times [-1/2, 1/2]$ using a grid containing two elements in the \tilde{x} -direction and 96 in the \tilde{z} -direction. Only two elements were required in the \tilde{x} -direction since the boundary conditions (27), (28) and (29) allow quasi-one-dimensional solutions in which all \tilde{x} derivatives of the solution vanish. Of the 96 elements in the \tilde{z} -direction, 32 were placed in the interval $-0.5 \leq \tilde{z} \leq -0.3$, 32 in the interval $-0.3 < \tilde{z} \leq 0.3$ and 32 in the interval $0.3 < \tilde{z} \leq 0.5$. This grid refinement was used since the charge density can possess steep gradients close to the bounding surfaces.

The computed solution for $\Gamma = 1$, $\sigma = 0.5$, $\varepsilon = 0.3$ and $\lambda = 115$ is shown in Figs 9(a)–(c) where we have taken a slice through our two-dimensional domain along the line $\tilde{x} = 0$. All other parallel slices are identical. For this value of ε , $\lambda_c \approx 32.9$. In Fig. 9(a) we have plotted the director angle θ against \tilde{z} . It can be seen that θ is symmetric about the mid-plane of the cell and the distorted solutions are qualitatively similar to the solutions obtained in the previous section, when a magnetic rather than an electrical field was applied. We have chosen the branch for which

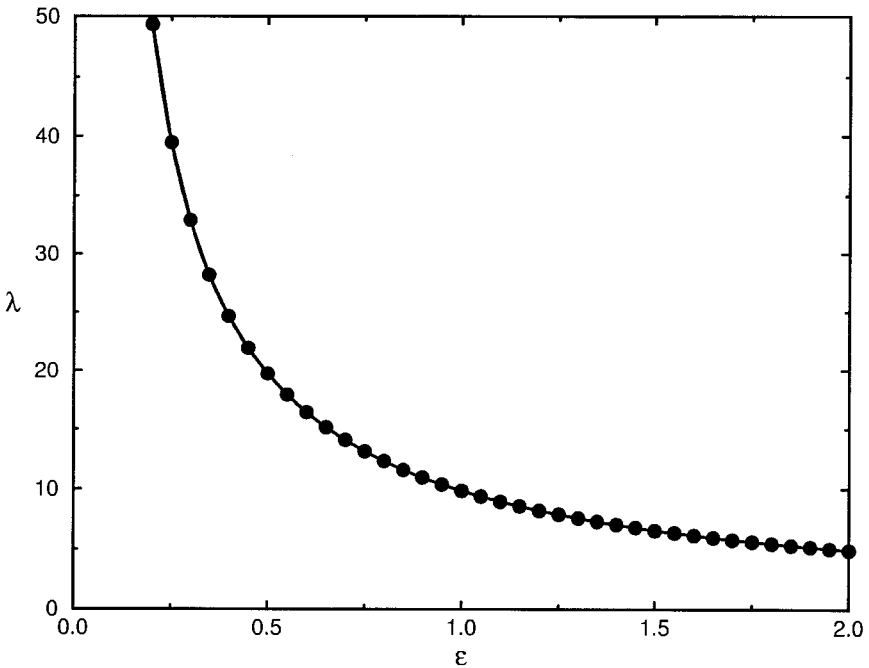


Fig. 8. Computed critical field strength λ_c against scaled dielectric susceptibility anisotropy ε . The solid line is $\lambda = \pi^2/\varepsilon$.

the director is rotated towards the bottom plate. The plot of θ against z along the other stable branch for the same values of the parameters can be obtained by reflecting Fig. 9(a) about $\theta = 0$. The charge density $\tilde{\rho}_e$ is plotted against z in Fig. 9(b). The charge density has extrema close to the boundaries of the cell where there is a build-up of charge, positive at one plate, and negative at the other. The rate of change of the electric potential in the z -direction ($\partial\tilde{\phi}/\partial z$) is plotted against z in Fig. 9(c). Plots of the charge density and rate of change of the electric potential along the other stable branch for the same values of the parameters are identical. The solution for the electric potential $\tilde{\phi}$ against z is only a slight perturbation from the linear profile that exists before the bifurcation occurs and is therefore not shown.

The profiles of θ , $\tilde{\rho}_e$ and $\partial\tilde{\phi}/\partial z$ along $x = 0$ are shown in Figs 10(a)–(c), respectively, for $\Gamma = 1$, $\sigma = 0.5$, $\varepsilon = 0.7$ and $\lambda = 75$ ($\lambda_c \approx 14.1$). The director rotation is again symmetric about $z = 0$ and we have again chosen the branch along which the director is rotated towards the bottom plate. The director rotation along the other stable branch can be obtained by reflection in $\theta = 0$. Notice that the sign of the charge density near the upper and lower plates in Fig. 10(b) is reversed compared to the case when $\varepsilon = 0.3$ shown in Fig. 9(b), while Figs 9(c) and 10(c) are qualitatively similar. Plots of $\tilde{\rho}_e$ and $\partial\tilde{\phi}/\partial z$ against z along the other stable branch at the same values of the parameters are identical to Figs 10(b) and (c).

For such quasi-one-dimensional solutions, equations (25) and (26) (after division by ε_\perp and σ_\perp , respectively) become

$$-\varepsilon \frac{\partial}{\partial z} \left(\frac{\partial \phi}{\partial z} \sin^2 \theta \right) = \frac{\partial^2 \phi}{\partial z^2} + \frac{\rho_e}{\varepsilon_0 \varepsilon_\perp}$$

and

$$-\sigma \frac{\partial}{\partial z} \left(\frac{\partial \phi}{\partial z} \sin^2 \theta \right) = \frac{\partial^2 \phi}{\partial z^2}$$

Hence

$$\frac{\varepsilon}{\sigma} = 1 + \frac{\rho_e}{\varepsilon_0 \varepsilon_{\perp} \phi_{zz}} \tag{41}$$

and immediately

$$\rho_e = 0 \text{ if } \frac{\varepsilon}{\sigma} = 1$$

$$\frac{\rho_e}{\phi_{zz}} > 0 \text{ if } \frac{\varepsilon}{\sigma} > 1$$

$$\frac{\rho_e}{\phi_{zz}} < 0 \text{ if } \frac{\varepsilon}{\sigma} < 1$$

This behaviour is independent of θ and is observed in Figs 9(b) and (c), and in Figs 10(b) and (c). In Fig. 9(b), $\tilde{\rho}_e$ is positive for $\tilde{z} < 0$ and negative for $\tilde{z} > 0$, while in Fig. 9(c), $\partial \tilde{\phi} / \partial \tilde{z}$ is a decreasing function for $\tilde{z} < 0$ and an increasing function for $\tilde{z} > 0$. Hence ρ_e and ϕ_{zz} have opposite sign, as is appropriate when $\varepsilon < \sigma$. A comparison of Figs 10(b) and (c) shows that ρ_e and ϕ_{zz} have the same sign, to be expected with $\varepsilon > \sigma$. When $\varepsilon = \sigma$, the computed charge density was identically zero as required.

5.2 Imperfect anchoring conditions

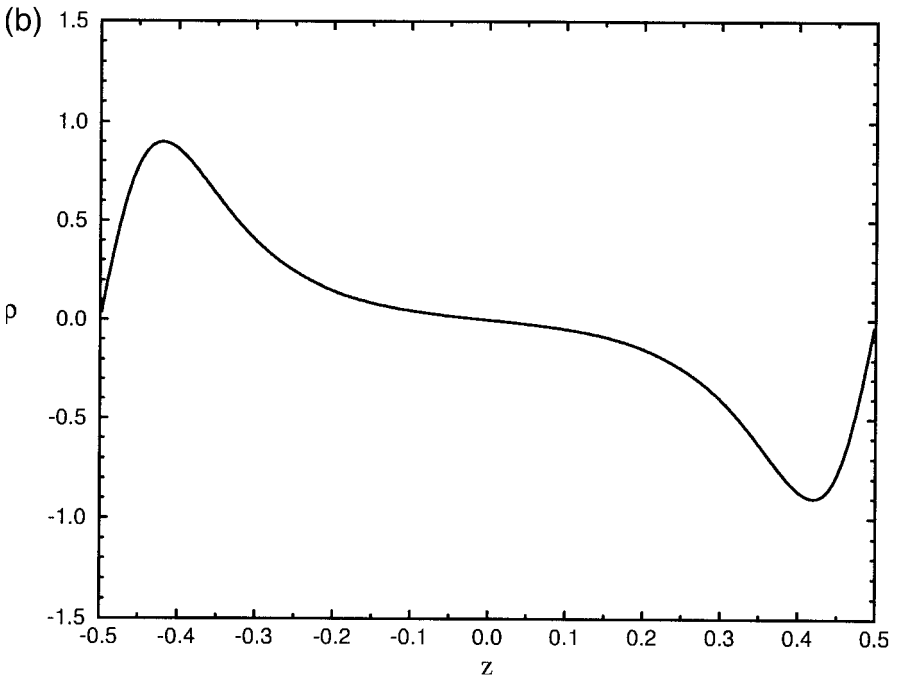
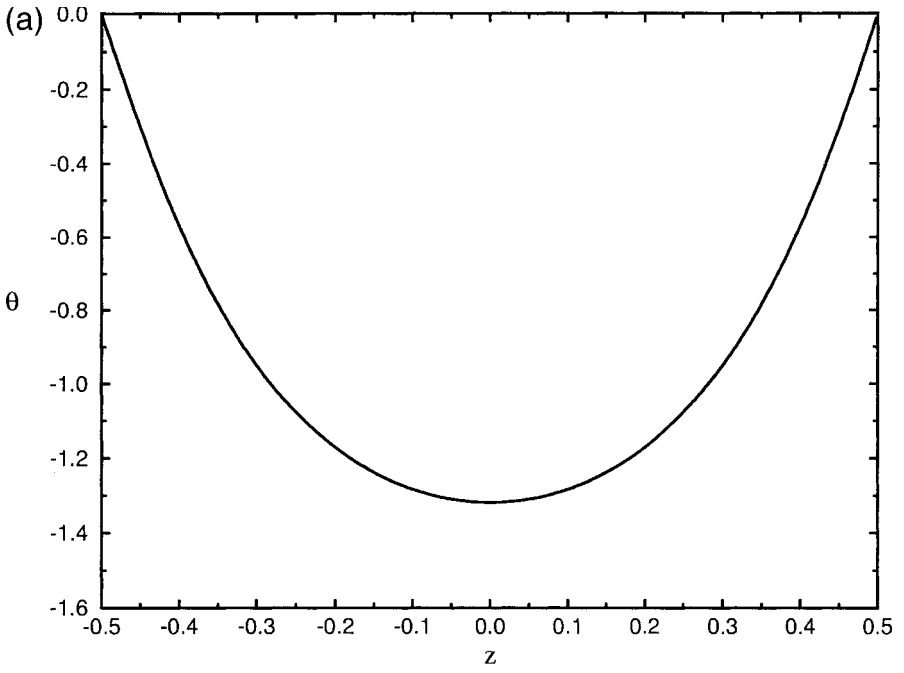
To introduce an imperfection into the system when an electric field is applied, a different approach is required from the magnetic field case. The simplest way to account for imperfections when an electric field is applied to the nematic slab is to assume that the alignment of the director is not perfect at one or both of the boundaries, and we introduce another parameter α to describe the misalignment at the bottom boundary. The boundary conditions at the bottom plate then read

$$\theta(\tilde{x}, -1/2) = \alpha, \quad -1/2 \leq \tilde{x} \leq 1/2 \tag{42}$$

These boundary conditions do not support Z_2 -invariant solutions, and in particular (39) is no longer a solution. The introduction of imperfection into the system leads to a disconnection of the pitchfork bifurcation and one obtains a diagram similar to Fig. 5. As the parameter α is increased or decreased the disconnection becomes larger or smaller accordingly and upon following the position of the limit point on the disconnected branch a cusp qualitatively similar to that of Fig. 7 is achieved. The position of the tip of the cusp, which occurs when $\alpha = 0$, varies with the value of ε and the cusp is again aligned with the λ -axis with vertical asymptotes at $\alpha = \pm \pi/2$.

5.3 Two-dimensional solutions

We now consider a truly two-dimensional version of the problem in which the gap has length l in the x -direction and in which we apply strong anchoring on the end walls such that there is homeotropic alignment at $x = \pm l/2$. In doing so we



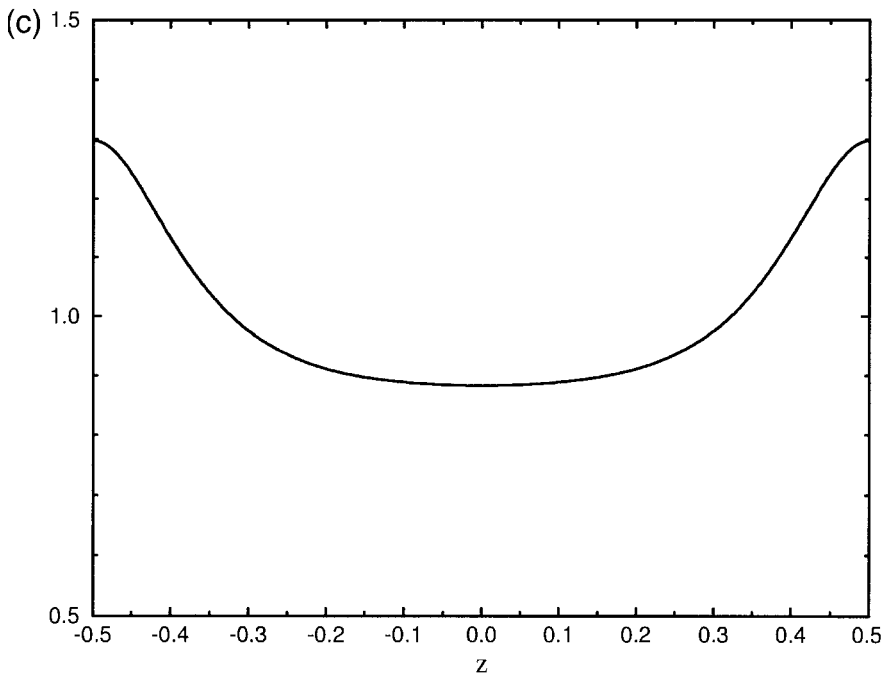


Fig. 9. Quasi-one-dimensional solution for $\Gamma = 1$, $\sigma = 0.5$, $\varepsilon = 0.3$ and $\lambda = 115$: (a) director angle $\theta(\tilde{z})$; (b) charge density $\tilde{\rho}_\varepsilon(\tilde{z})$; (c) rate of change of electric potential $(\partial\tilde{\psi}/\partial\tilde{z})(\tilde{z})$.

destroy the quasi-one-dimensional behaviour observed above. We retain boundary conditions (36) and (37), but on $\tilde{x} = \pm 1/2$ we apply

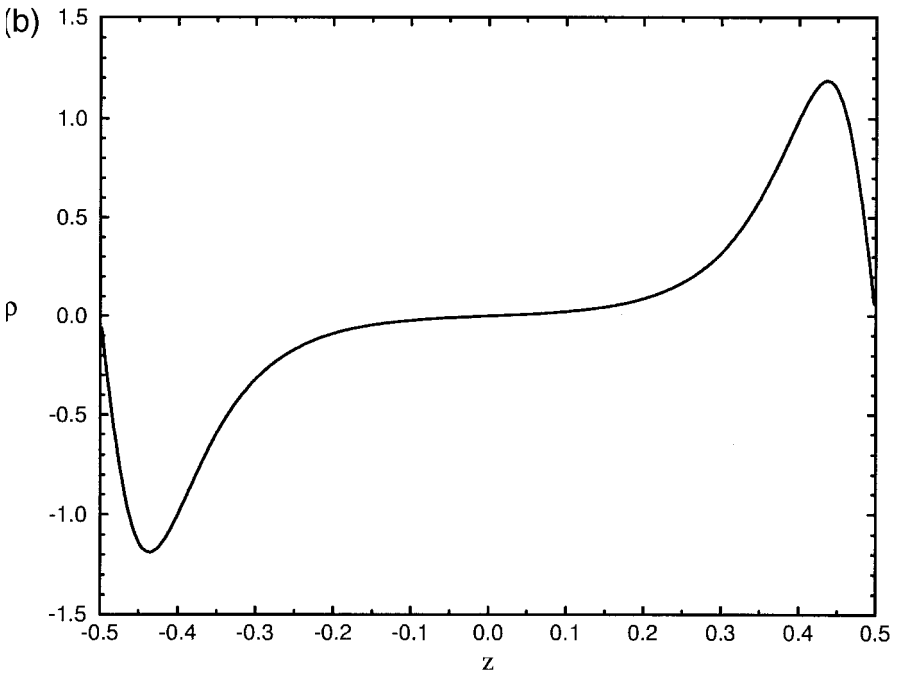
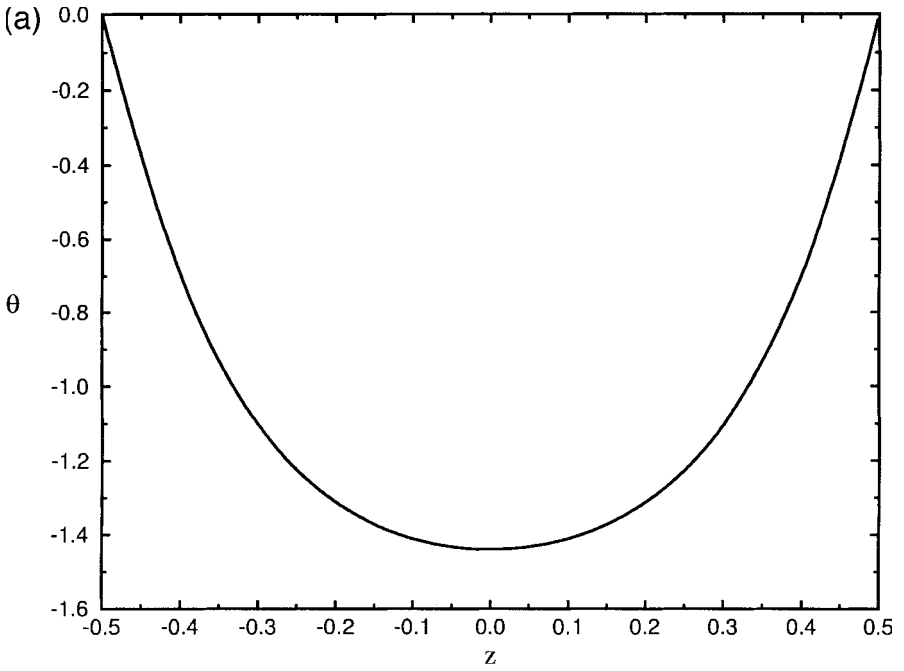
$$\begin{aligned} \theta(-1/2, \tilde{z}) &= \frac{\partial\tilde{\rho}_\varepsilon}{\partial\tilde{x}}(-1/2, \tilde{z}) = \frac{\partial\tilde{\psi}}{\partial\tilde{x}}(-1/2, \tilde{z}) = \theta(1/2, \tilde{z}) \\ &= \frac{\partial\tilde{\rho}_\varepsilon}{\partial\tilde{x}}(1/2, \tilde{z}) = \frac{\partial\tilde{\psi}}{\partial\tilde{x}}(1/2, \tilde{z}) = 0 \end{aligned} \tag{43}$$

for $-1/2 < \tilde{z} < 1/2$. These boundary conditions support Z_2 -invariant solutions of the governing equations and the Freedericksz transition again occurs at a Z_2 -symmetry breaking bifurcation point. The critical value of the electric field at which the transition occurs is now a function of the aspect ratio Γ , and in Fig. 11 for $\sigma = \varepsilon = 0.5$, we see that λ_c approaches the value π^2/ε (the dashed line in Fig. 11) as Γ increases, as is expected.

Plots of the director orientation, normalized charge density and electric potential are shown for $\Gamma = 1$, $\sigma = 0.5$, $\varepsilon = 0.3$, $\lambda = 97.5$ and $\Gamma = 1$, $\sigma = 0.5$, $\varepsilon = 0.7$, $\lambda = 38.5$ in Figs 12(a)–(c) and 13(a)–(c), respectively. These solutions were computed using 32×32 quadrilateral elements with biquadratic interpolation of the angle, charge density and electric potential on each element. In both figures, the contours of θ are equally spaced between 0 and 0.7, the contours of $\tilde{\rho}_\varepsilon$ are equally spaced between -0.35 and 0.35 , and the contours of $\tilde{\psi}$ are equally spaced between -0.5 and 0.5 .

By a similar argument to that above

$$\frac{\varepsilon}{\sigma} = 1 + \frac{\rho_\varepsilon}{\varepsilon_0 \varepsilon_\perp (\phi_{xx} + \phi_{zz})} \tag{44}$$



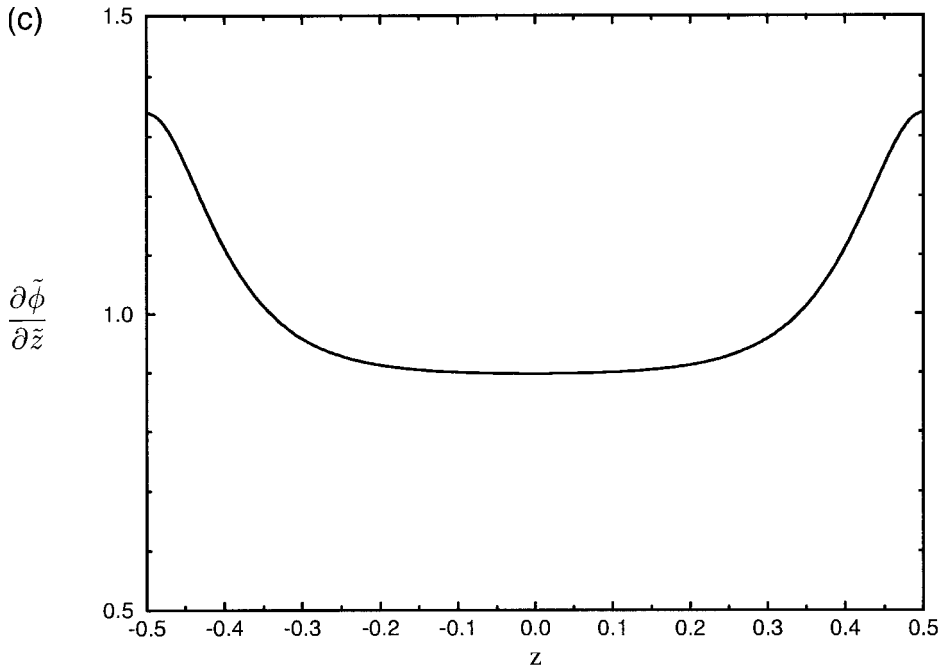


Fig. 10. Quasi-one-dimensional solution for $\Gamma = 1$, $\sigma = 0.5$, $\varepsilon = 0.7$ and $\lambda = 75$: (a) director angle $\theta(z)$; (b) charge density $\tilde{\rho}_i(z)$; (c) rate of change of electric potential $(\frac{\partial \tilde{\phi}}{\partial \tilde{z}})(z)$.

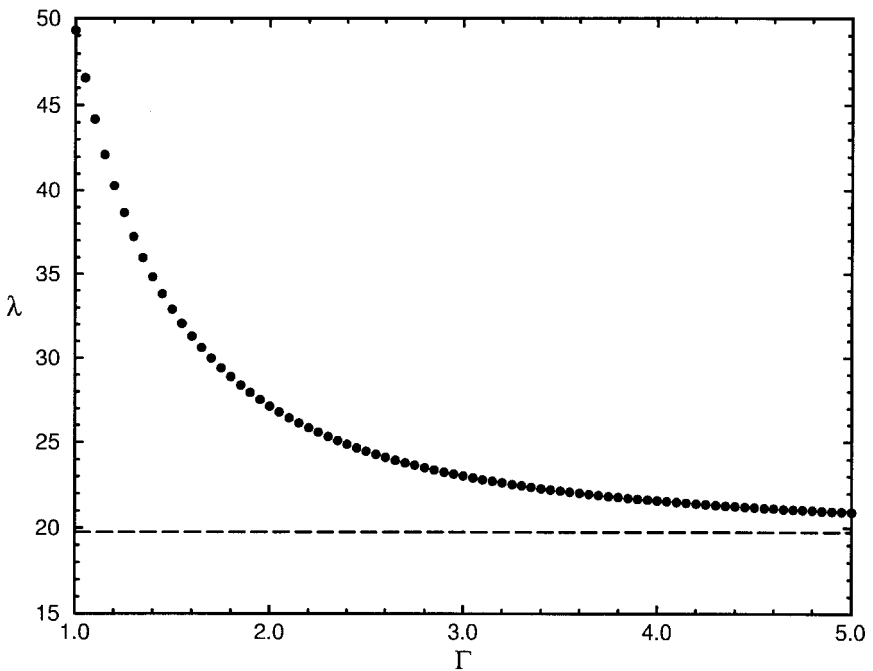
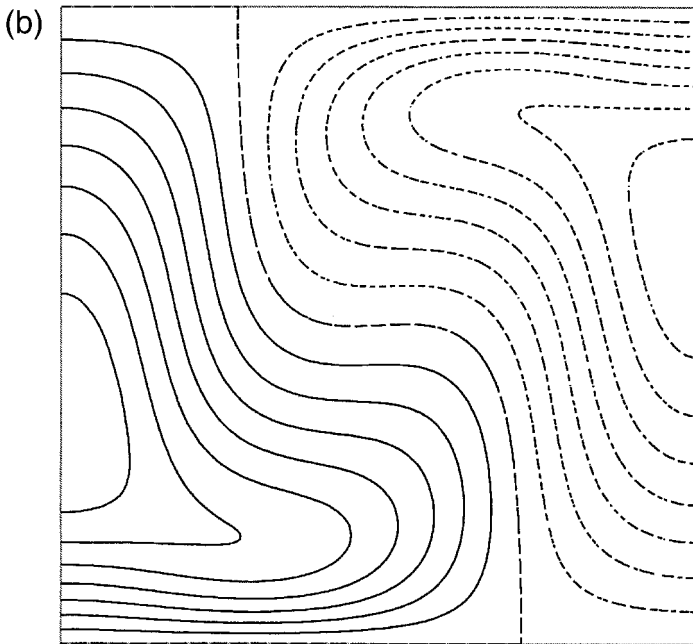
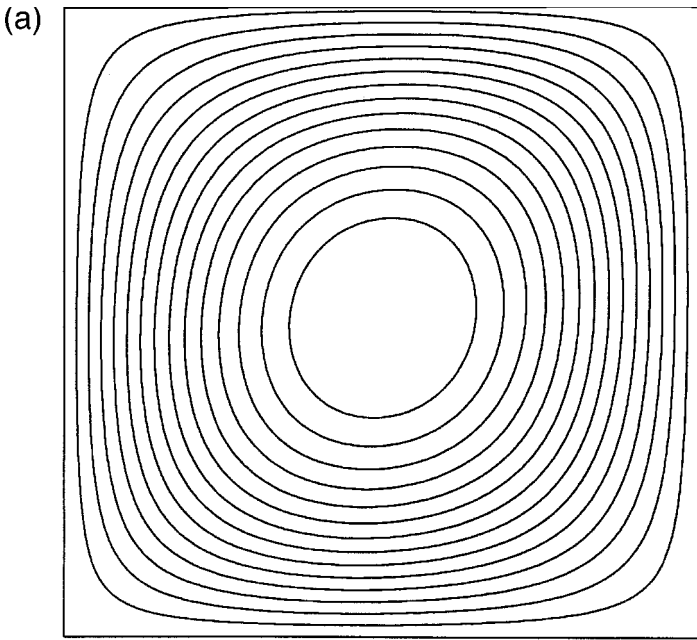


Fig. 11. Critical field strength λ_c against aspect ratio Γ for $\sigma = \varepsilon = 0.5$. The horizontal dashed line is $\lambda = \pi^2/\varepsilon$.



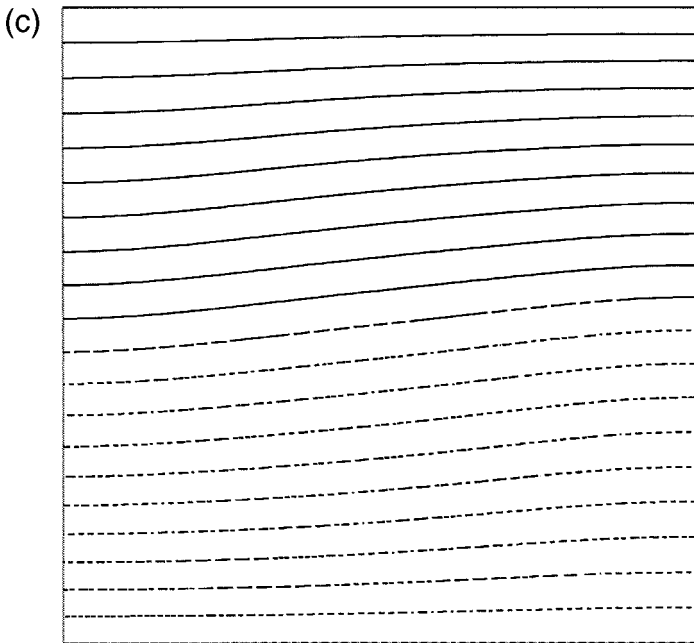


Fig. 12. Two-dimensional solution for $\Gamma = 1$, $\sigma = 0.5$, $\varepsilon = 0.3$, $\lambda = 97.5$, and $(x, z) \in [-1/2, 1/2] \times [-1/2, 1/2]$. (a) Director angle $\theta(x, z)$. Contours are equally spaced between 0 and 0.7. (b) Charge density $\tilde{\rho}_e(x, z)$. Contours are equally spaced between -0.35 and 0.35 . (c) Electric potential $\tilde{\phi}(x, z)$. Contours are equally spaced between -0.5 and 0.5 .

hence

$$\rho_e = 0 \text{ if } \frac{\varepsilon}{\sigma} = 1$$

$$\frac{\rho_e}{(\phi_{xx} + \phi_{zz})} > 0 \text{ if } \frac{\varepsilon}{\sigma} > 1$$

$$\frac{\rho_e}{(\phi_{xx} + \phi_{zz})} < 0 \text{ if } \frac{\varepsilon}{\sigma} < 1$$

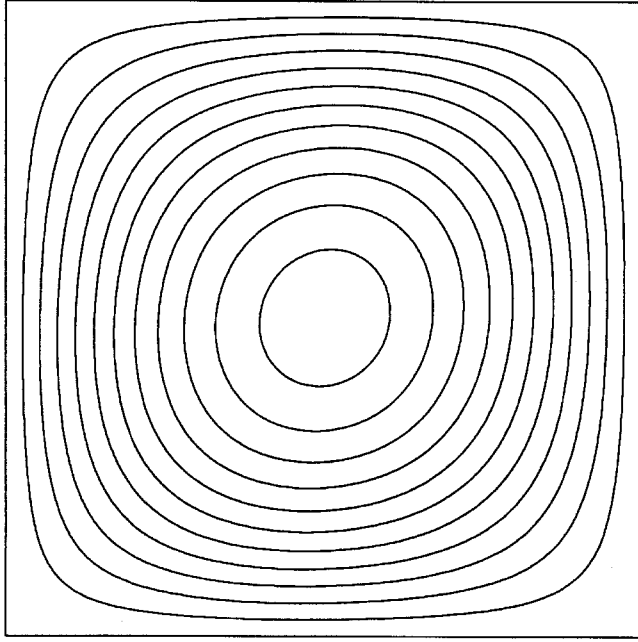
Any perturbations to the boundary conditions which do not allow symmetric solutions disconnect the pitchfork bifurcation point as for the one-dimensional case.

6 Conclusions

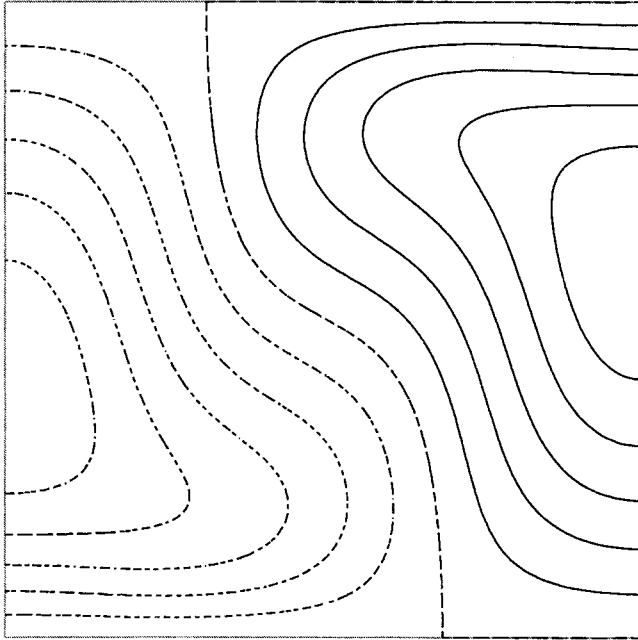
We have successfully applied ideas from singularity theory coupled with numerical bifurcation methods to explore the static instability known as the Fredericksz transition in nematic liquid crystal. The effects of both magnetic and electric fields have been considered and we have also investigated the physically relevant situations where imperfections are present. This approach has allowed us to uncover important details of the mechanisms involved such as the charge distributions. These are difficult to explore in the laboratory because of the small length scales involved and have defied previous analytic approaches.

The detailed numerical investigation of such complex materials is of significant

(a)



(b)



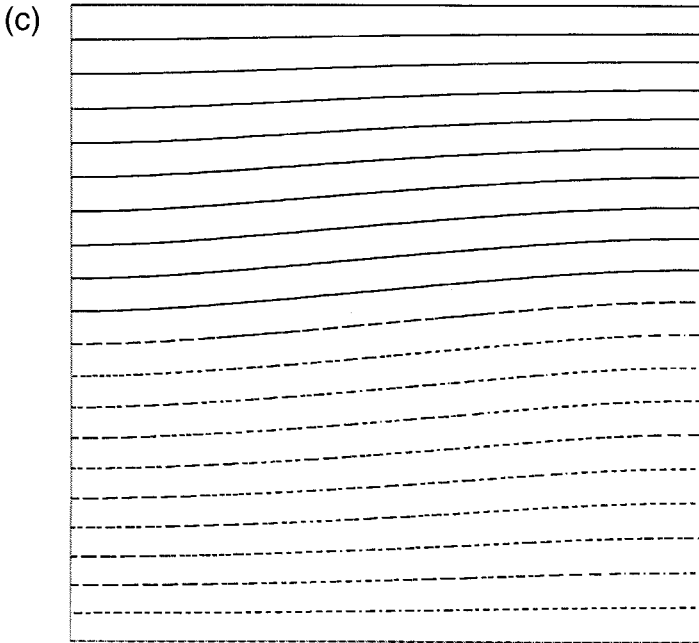


Fig. 13. Two-dimensional solution for $\Gamma = 1$, $\sigma = 0.5$, $\varepsilon = 0.7$, $\lambda = 38.5$, and $(x, z) \in [-1/2, 1/2] \times [-1/2, 1/2]$. (a) Director angle $\theta(x, z)$. Contours are equally spaced between 0 and 0.7. (b) Charge density $\bar{\rho}_e(x, z)$. Contours are equally spaced between -0.35 and 0.35 . (c) Electric potential $\bar{\phi}(x, z)$. Contours are equally spaced between -0.5 and 0.5 .

practical relevance since the Freedericksz transition is important in device applications. Hence we now have a powerful numerical tool which can readily be used to investigate the effects of material properties for example. We have already initiated such an investigation and considered the case where the dielectric anisotropy $\Delta\varepsilon < 0$. Here electrohydrodynamic convection occurs in the cell and the induced flow has been considered. The basic mechanism for this effect is the motion of ions through the cell. This situation is beyond the scope of this paper but our ability to calculate the director profile, the electric potential and the distribution of charge in the cell for $\Delta\varepsilon > 0$ is encouraging.

Acknowledgements

The authors are grateful to Andrew Cliffe for useful discussions. GIB would like to thank the Leverhulme Trust for financial support. SJT acknowledges the financial support from NFS grant DMS-9704714. This work was undertaken whilst SJT was visiting the Computing Laboratory at Oxford University.

References

Benjamin, T. B. (1978) Bifurcation phenomena in steady flows of a viscous liquid. part i. theory. *Proceedings of the Royal Society London A* **337**, 1–26.
 Brenner, S. C. and Scott, L. R. (1994) *The Mathematical Theory of Finite Element Methods* (Springer-Verlag, New York).

- Cliffe, K. A. (1996) Entwife (release 6.3) reference manual: Entwife, initial data and solver data commands, AEAT-0823.
- Cliffe, K. A. and Winters, K. H. (1984) A numerical study of the cusp catastrophe for Bénard convection in tilted cavities. *J. Comp. Phys.* **54**, 531–534.
- Dafermos, C. M. (1968) Stability of orientation patterns of liquid crystals subject to magnetic fields. *SIAM Journal of Applied Mathematics* **16**, 1305–1318.
- de Gennes, P. G. and Prost, J. (1993) *The Physics of Liquid Crystals* (Oxford University Press, Oxford).
- Derfel, G. (1988) Field effects in nematic liquid crystals in terms of catastrophe theory. *Liquid Crystals* **93**, 1411–1424.
- Deuling, H. J. (1972) Deformation of nematic liquid crystals in an electric field. *Mol. Cryst. Liq. Cryst.* **19**, 123–131.
- Deuling, H. J. (1978) Elasticity of nematic liquid crystals. *Solid State Physics Supplement*, Vol. 14 (ed. L. Liebert; Academic Press, London), pp. 77–107.
- Dunmur, D. and Toriyama, K. (1998) Elastic properties. *Handbook of Liquid Crystals*, Vol. 1 (eds J. Goodby, G. W. Gray and H. W. Spiess; Wiley, New York), pp. 253–280.
- Eriksen, J. L. (1966) Inequalities in liquid crystal theory. *Physics of Fluids* **9**, 1205–1207.
- Frank, F. C. (1958) On the theory of liquid crystals. *Discussions of the Faraday Society* **25**, 19–28.
- Golubitsky, M. and Schaeffer, D. G. (1985) *Singularities and Groups in Bifurcation Theory*, Vol. I (Springer-Verlag, New York).
- Gruler, H. and Meier, G. (1972) Electric field-induced deformations in oriented liquid crystals of the nematic type. *Mol. Cryst. Liq. Cryst.* **16**, 299–310.
- Kaiser, E. and Pesch, W. (1993) Amplitude equations for the electrohydrodynamic instability in nematic liquid crystals. *Physical Review E* **48**, 4510–4528.
- Keller, H. B. (1977) Numerical solution of bifurcation and nonlinear eigenvalue problems. *Applications of Bifurcation Theory* (ed. P. H. Rabinowitz; Academic Press, New York), pp. 359–384.
- Leslie, F. M. (1970) Distortion of twisted orientation patterns in liquid crystals by magnetic fields. *Mol. Cryst. Liq. Cryst.* **12**, 57–72.
- Leslie, F. M. (1970) Some magneto-hydrostatic effects in nematic liquid crystals. *Journal of Physics D: Applied Physics* **3**, 889–897.
- Leslie, F. M. (1992) Continuum theory for nematic liquid crystals. *Continuum Mechanics Thermo-dynamics* **4**, 167–175.
- Moore, G. and Spence, A. (1980) The calculation of turning points of nonlinear equations. *SIAM Journal of Numerical Analysis* **17**, 567–576.
- Mullin, T. (1995) *The Nature of Chaos* (Clarendon Press, Oxford).
- Mullin, T. and Kobine, J. J. (1996) Organised chaos in fluid dynamics. *Nonlinear Mathematics and its Applications* (ed. P. Aston; Cambridge University Press, London).
- Saupe, A. (1960) Die biegeelastizität der nematischen phase von azoxyanisol. *Zeitschrift für Naturforschung* **15a**, 815–822.
- Schiller, P. (1989) Perturbation theory for planar nematic twisted layers. *Liquid Crystals* **4**, 69–78.
- Werner, B. and Spence, A. (1984) The computation of symmetry breaking bifurcation points. *SIAM Journal of Numerical Analysis* **21**, 388–399.

Appendix A. Freedericksz transition applying a magnetic field

The problem described has a reflectional (anti)symmetry about the mid-plane parallel to the bounding surfaces when $\psi = 0$. Consider the balance of torque equation (15), which we write as

$$\begin{aligned}
 F(\theta; H) = & K_1 \left(\frac{d^2\theta}{dz^2} \cos \theta - \left(\frac{d\theta}{dz} \right)^2 \sin \theta \right) \cos \theta \\
 & + K_3 \left(\frac{d^2\theta}{dz^2} \sin \theta + \left(\frac{d\theta}{dz} \right)^2 \cos \theta \right) \sin \theta \\
 & + \Delta\chi H^2 \sin(\theta + \psi) \cos(\theta + \psi) = 0
 \end{aligned} \tag{A1}$$

where $\theta(z)$ has the necessary smoothness. We now show that for $\psi = 0$

$$SF(\theta; H) = F(S\theta; H) \quad (\text{A2})$$

for the reflection operator

$$S\theta(z) = -\theta(-z) \quad (\text{A3})$$

i.e. F is equivariant with respect to a symmetry operator $S \neq I$ such that $S^2 = I$.

Note that

$$\frac{d}{dz}[S\theta] = \frac{d}{dz}[-\theta(-z)] = \frac{d}{dz}[\theta(-z)], \quad \frac{d^2}{dz^2}[S\theta] = -\frac{d^2}{dz^2}[\theta(-z)]$$

$$\cos[S\theta] = \cos[-\theta(-z)] = \cos[\theta(-z)], \quad \sin[S\theta] = \sin[-\theta(-z)] = -\sin[\theta(-z)]$$

hence

$$\begin{aligned} F(S\theta; H) &= K_1 \left(-\frac{d^2\theta}{dz^2} \cos \theta + \left(\frac{d\theta}{dz} \right)^2 \sin \theta \right) \cos \theta \\ &\quad - K_3 \left(\frac{d^2\theta}{dz^2} \sin \theta + \left(\frac{d\theta}{dz} \right)^2 \cos \theta \right) \sin \theta - \Delta\chi H^2 \sin \theta \cos \theta \end{aligned}$$

and

$$\begin{aligned} SF(\theta; H) &= -K_1 \left(\frac{d^2\theta}{dz^2} \cos \theta - \left(\frac{d\theta}{dz} \right)^2 \sin \theta \right) \cos \theta \\ &\quad - K_3 \left(\frac{d^2\theta}{dz^2} \sin \theta + \left(\frac{d\theta}{dz} \right)^2 \cos \theta \right) \sin \theta - \Delta\chi H^2 \sin \theta \cos \theta \end{aligned}$$

Clearly

$$\cos[S\theta + \psi] = \cos[-\theta(-z) + \psi] \neq \cos[\theta(-z) + \psi]$$

$$\sin[S\theta + \psi] = \sin[-\theta(-z) + \psi] \neq -\sin[\theta(-z) + \psi]$$

so equation (A1) is equivariant with respect to S if and only if $\psi = 0$.

Boundary conditions (16) support Z_2 -invariant solutions, i.e. solutions that are invariant under the action of S .

Now consider the non-dimensionalized weak form (20) which we write as

$$\begin{aligned} a(\theta; \Theta, \lambda) &= \int_{-1/2}^{1/2} \left\{ \left[(\mu - 1) \left(\frac{d\theta}{dz} \right)^2 \sin \theta \cos \theta + \lambda \sin(\theta + \psi) \cos(\theta + \psi) \right] \Theta \right. \\ &\quad \left. - (\cos^2 \theta + \mu \sin^2 \theta) \frac{d\theta}{dz} \frac{d\Theta}{dz} \right\} dz = 0 \end{aligned} \quad (\text{A4})$$

where $\theta(z)$, $\Theta(z) \in V$, the Hilbert space of functions whose (generalized) first derivatives are square integrable over the interval $[-1/2, 1/2]$ and whose function values vanish at $z = \pm 1/2$.

Applying the Riesz Representation Theorem (Brenner and Scott, 1994), we now define the operator

$$A : V \times \mathbb{R} \mapsto V$$

by

$$A(\theta; \lambda) = Q \text{ where } a(\theta; \Theta, \lambda) = \langle Q, \Theta \rangle \forall \Theta \in V \quad (\text{A5})$$

and $\langle \cdot, \cdot \rangle$ denotes the inner product. At a solution of (A1), we have

$$A(\theta; \lambda) = 0 \quad (\text{A6})$$

Now, we more carefully define the symmetry operator (A3) as

$$S : V \mapsto V$$

by

$$S\theta(\mathbf{z}) = -\theta(-\mathbf{z}) \quad (\text{A7})$$

from (A4)

$$a(S\theta; \Theta, \lambda) = a(\theta; S\Theta, \lambda) \quad (\text{A8})$$

if and only if $\psi = 0$. Further, by definition of $\langle \cdot, \cdot \rangle$

$$\langle Sa, b \rangle = \langle a, Sb \rangle \forall a, b \in V \quad (\text{A9})$$

From (A5)

$$SA(\theta; \lambda) = SQ \text{ where } a(\theta; \Theta, \lambda) = \langle Q, \Theta \rangle \forall \Theta \in V$$

Define

$$A(S\theta; \lambda) = P \text{ where } a(S\theta; \Theta, \lambda) = \langle P, \Theta \rangle \forall \Theta \in V$$

Now

$$\langle P, \Theta \rangle = a(S\theta; \Theta, \lambda) \forall \Theta \in V = a(\theta; S\Theta, \lambda)$$

by (A8), so

$$\langle P, \Theta \rangle = \langle Q, S\Theta \rangle \forall \Theta \in V = \langle SQ, \Theta \rangle \quad (\text{A10})$$

by (A9). Hence

$$P = SQ$$

and we have

$$SA(\theta; \lambda) = A(S\theta; \lambda)$$

That is, the operator A is equivariant with respect to S .

Finally, upon discretization of (20) we have

$$a_h(\theta_h; \Theta_h, \lambda) = \int_{-1/2}^{1/2} \left\{ \left[(\mu - 1) \left(\frac{d\theta_h}{d\mathbf{z}} \right)^2 \sin \theta_h \cos \theta_h + \lambda \sin(\theta_h + \psi) \cos(\theta_h + \psi) \right] \Theta_h \right. \\ \left. - (\cos^2 \theta_h + \mu \sin^2 \theta_h) \frac{d\theta_h}{d\mathbf{z}} \frac{d\Theta_h}{d\mathbf{z}} \right\} d\mathbf{z} \quad (\text{A11})$$

where $\theta_h(\tilde{z}), \Theta_h(\tilde{z}) \in V_h \subset V$ and V_h is finite dimensional. Define the operator

$$A_h : V_h \times \mathbb{R} \mapsto V_h$$

by

$$A_h(\theta_h; \lambda) = Q_h \text{ where } a_h(\theta_h; \Theta_h, \lambda) = \langle Q_h, \Theta_h \rangle \forall \Theta_h \in V_h \tag{A12}$$

and $\langle \cdot, \cdot \rangle$ is the inner product. At a solution of (A1), we have

$$A_h(\theta_h; \lambda) = 0 \tag{A13}$$

Provided the finite-dimensional subspace V_h is constructed so that the symmetry operator S maps V_h on to itself, that is

$$S : V_h \mapsto V_h \tag{A14}$$

then

$$a_h(S\theta_h; \Theta_h, H) = a_h(\theta_h; S\Theta_h, H)$$

A finite-dimensional subspace V_h that is invariant under the reflection operator S can be ensured by constructing a finite-element mesh that is symmetric about $\tilde{z} = 0$. Since

$$\langle SQ_h, \Theta_h \rangle = \langle Q_h, S\Theta_h \rangle$$

by repeating the previous argument we have

$$SA_h(\theta_h; \lambda) = A_h(S\theta_h; \lambda) \tag{A15}$$

The operator A_h is also equivariant with respect to S .

Now let

$$\theta_h(\tilde{z}) \in V_h = \sum_{i=1}^n u_i \psi_i(\tilde{z}) \tag{A16}$$

where $\psi_i(\tilde{z}), i = 1, \dots, n$ form a basis for V_h . Assuming that the space V_h spanned by $\psi_i(\tilde{z}), i = 1, \dots, n$ is invariant with respect to S , i.e. that equation (A14) is satisfied, and numbering basis functions ψ_i such that

$$S\psi_i = -\psi_{n+1-i}$$

then for any $\theta_h \in V_h$

$$S\theta_h = \sum_{i=1}^n -u_{n+1-i} \psi_i \tag{A17}$$

Defining the vector \mathbf{u} by

$$\mathbf{u} = [(u_i)]_{i=1, \dots, n}$$

this can be written as

$$\hat{S}\mathbf{u} = \begin{pmatrix} 0 & 0 & \dots & 0 & -1 \\ 0 & 0 & \dots & -1 & 0 \\ \vdots & \vdots & & \vdots & \vdots \\ 0 & -1 & \dots & 0 & 0 \\ -1 & 0 & \dots & 0 & 0 \end{pmatrix} \mathbf{u}$$

where \hat{S} is a finite-dimensional representation of S on V_h . Defining

$$f_i = \langle A_h(\theta_h, \lambda), \psi_i \rangle, i = 1, \dots, n$$

equation (A13) becomes

$$\mathbf{f}(\mathbf{u}, \lambda) = \mathbf{0} \tag{A18}$$

Further, since

$$f_i(\hat{S}\mathbf{u}, \lambda) = \langle P_h, \psi_i \rangle = \langle Q_h, S\psi_i \rangle$$

by (A10), then

$$f_i(\hat{S}\mathbf{u}, \lambda) = \langle Q_h, -\psi_{n+1-i} \rangle = -f_{n+1-i}(\mathbf{u}, \lambda)$$

Thus

$$\mathbf{f}(\hat{S}\mathbf{u}, \lambda) = \hat{S}\mathbf{f}(\mathbf{u}, \lambda) \tag{A19}$$

where $\hat{S} \neq I$ and $\hat{S}^2 = I$. Therefore, we see that the non-linear algebraic system of equations (A18) is also Z_2 -equivariant.

Appendix B. Fredericksz transition applying an electrical field

The coupled system of equations governing the equilibrium of a nematic liquid crystal in the presence of an applied electrical field is also Z_2 -equivariant. Let

$$\mathbf{t}(x, z) = \begin{pmatrix} \theta(x, z) \\ \phi(x, z) \\ \rho_e(x, z) \end{pmatrix} \tag{B1}$$

and write equations (24)–(26) as

$$\mathbf{G}(\mathbf{t}) = \begin{pmatrix} G_1(\mathbf{t}) \\ G_2(\mathbf{t}) \\ G_3(\mathbf{t}) \end{pmatrix} = \mathbf{0}$$

We now show that

$$\mathbf{S}\mathbf{G}(\mathbf{t}) = \mathbf{G}(\mathbf{S}\mathbf{t}) \tag{B2}$$

where \mathbf{S} is the reflection operator

$$\mathbf{S} \begin{pmatrix} \theta(x, z) \\ \phi(x, z) \\ \rho_e(x, z) \end{pmatrix} = \begin{pmatrix} -\theta(x, -z) \\ -\phi(x, -z) \\ -\rho_e(x, -z) \end{pmatrix} \tag{B3}$$

or

$$\mathbf{S}\mathbf{t}(x, z) = -\mathbf{t}(x, -z)$$

Note that

$$\frac{\partial}{\partial x}[\mathbf{St}] = \frac{\partial}{\partial x}[-\mathbf{t}(x, -z)] = -\frac{\partial}{\partial x}[\mathbf{t}(x, -z)], \quad \frac{\partial^2}{\partial x^2}[\mathbf{St}] = -\frac{\partial^2}{\partial x^2}[\mathbf{t}(x, -z)]$$

$$\frac{\partial}{\partial z}[\mathbf{St}] = \frac{\partial}{\partial z}[-\mathbf{t}(x, -z)] = \frac{\partial}{\partial z}[\mathbf{t}(x, -z)], \quad \frac{\partial^2}{\partial z^2}[\mathbf{St}] = -\frac{\partial^2}{\partial z^2}[\mathbf{t}(x, -z)]$$

hence

$$\begin{aligned} G_1(\mathbf{St}) &= -K(-\theta_{xx} - \theta_{zz}) \\ &\quad + \Delta\varepsilon(-\phi_x \cos \theta - \phi_z \sin \theta)(\phi_x \sin \theta - \phi_z \cos \theta) \\ G_2(\mathbf{St}) &= \varepsilon_{\perp}(\theta_{xx} + \theta_{zz}) - \Delta\varepsilon \frac{\partial}{\partial x} [(-\phi_x \cos \theta - \phi_z \sin \theta) \cos \theta] \\ &\quad - \Delta\varepsilon \frac{\partial}{\partial z} [(-\phi_x \cos \theta - \phi_z \sin \theta) \sin \theta] + \frac{\rho_e}{\varepsilon_0} \\ G_3(\mathbf{St}) &= \sigma_{\perp}(\theta_{xx} + \theta_{zz}) - \Delta\sigma \frac{\partial}{\partial x} [(-\phi_x \cos \theta - \phi_z \sin \theta) \cos \theta] \\ &\quad - \Delta\sigma \frac{\partial}{\partial z} [(-\phi_x \cos \theta - \phi_z \sin \theta) \sin \theta] \end{aligned}$$

and

$$\begin{aligned} (\mathbf{SG})_1(\mathbf{t}) &= K(\theta_{xx} + \theta_{zz}) - \Delta\varepsilon(\phi_x \cos \theta + \phi_z \sin \theta)(\phi_x \sin \theta - \phi_z \cos \theta) \\ (\mathbf{SG})_2(\mathbf{t}) &= -\varepsilon_{\perp}(-\theta_{xx} - \theta_{zz}) + \Delta\varepsilon \frac{\partial}{\partial x} [(\phi_x \cos \theta + \phi_z \sin \theta) \cos \theta] \\ &\quad + \Delta\varepsilon \frac{\partial}{\partial z} [(\phi_x \cos \theta + \phi_z \sin \theta) \sin \theta] + \frac{\rho_e}{\varepsilon_0} \\ (\mathbf{SG})_3(\mathbf{t}) &= -\sigma_{\perp}(-\theta_{xx} - \theta_{zz}) + \Delta\sigma \frac{\partial}{\partial x} [(\phi_x \cos \theta + \phi_z \sin \theta) \cos \theta] \\ &\quad + \Delta\sigma \frac{\partial}{\partial z} [(\phi_x \cos \theta + \phi_z \sin \theta) \sin \theta] \end{aligned}$$

where

$$\mathbf{SG}(t) = \begin{pmatrix} (\mathbf{SG})_1(t) \\ (\mathbf{SG})_2(t) \\ (\mathbf{SG})_3(t) \end{pmatrix} \tag{B4}$$

All the arguments applied to the previous scalar case can be suitably modified for this vector case.